Neuron
Article

A Cluster of Cholinergic Premotor Interneurons Modulates Mouse Locomotor Activity

Laskaro Zagoraiou,[1] Turgay Akay,[1] James F. Martin,[2] Robert M. Brownstone,[3] Thomas M. Jessell,[1,*] and Gareth B. Miles[4]
[1]Howard Hughes Medical Institute, Kavli Institute for Brain Science, Departments of Neuroscience and Biochemistry and Molecular Biophysics, Columbia University, New York, NY 10032, USA
[2]Institute of Biosciences and Technology, Texas A&M System Health Science Center, Houston, TX 77030, USA
[3]Departments of Surgery and Anatomy and Neurobiology, Neuroscience Institute, Dalhousie University, Halifax B3H 1X5, Canada
[4]School of Biology, University of St Andrews, St Andrews, Fife KY169TS, UK
*Correspondence: tmj1@columbia.edu
DOI 10.1016/j.neuron.2009.10.017

SUMMARY

Mammalian motor programs are controlled by networks of spinal interneurons that set the rhythm and intensity of motor neuron firing. Motor neurons have long been known to receive prominent "C bouton" cholinergic inputs from spinal interneurons, but the source and function of these synaptic inputs have remained obscure. We show here that the transcription factor Pitx2 marks a small cluster of spinal cholinergic interneurons, $V0_C$ neurons, that represents the sole source of C bouton inputs to motor neurons. The activity of these cholinergic interneurons is tightly phase locked with motor neuron bursting during fictive locomotor activity, suggesting a role in the modulation of motor neuron firing frequency. Genetic inactivation of the output of these neurons impairs a locomotor task-dependent increase in motor neuron firing and muscle activation. Thus, $V0_C$ interneurons represent a defined class of spinal cholinergic interneurons with an intrinsic neuromodulatory role in the control of locomotor behavior.

INTRODUCTION

Motor behaviors are constructed and constrained by neural circuits that coordinate the activation of skeletal muscles. The immediate task of regulating the limb muscles that control many aspects of vertebrate locomotor behavior has been assigned to circuits in the spinal cord, and in particular to networks of interneurons that determine the temporal dynamics of motor neuron activation. Elemental features of locomotion—the rhythm and pattern of motor neuron firing—are controlled by sets of excitatory and inhibitory interneurons that use fast-acting amino acid transmitters (Hochman and Schmidt, 1998; Cazalets et al., 1996; Shefchyk and Jordan, 1985; Fetcho et al., 2008; Orsal et al., 1986). Locomotor programs can also undergo adaptive changes in response to the biomechanical demands of particular motor tasks (Gillis and Biewener, 2001). These context-dependent features of locomotion involve moment-by-moment changes in the frequency of firing of spinal motor neurons, usually triggered by slower-acting modulatory networks of supraspinal and intraspinal origin (Jordan et al., 2008; Grillner, 2006). Much has been learned about the organization and function of descending modulatory systems, but the identity, connectivity, and physiological roles of intrinsic spinal modulatory interneurons have been more difficult to untangle.

In many regions of the CNS, modulatory influences on neuronal output and behavior are mediated by sets of cholinergic interneurons that elicit a diverse array of postsynaptic responses. The activation of cortical cholinergic systems modulates sensory threshold, states of attention, and the consolidation of memory (Pauli and O'Reilly, 2008; Giocomo and Hasselmo, 2007; Lawrence, 2008). In subcortical regions, cholinergic interneurons regulate the output of dopaminergic pathways implicated in sensory-motor learning, action selection, and reward (Mena-Segovia et al., 2008; Joshua et al., 2008; Wang et al., 2006; Maskos et al., 2005). Many of these insights into cholinergic modulatory function have emerged through pharmacological manipulation of cholinergic receptor systems, although the widespread distribution of most receptors (Wess, 2003) has made it difficult to establish a clear link between the dynamics of cholinergic microcircuitry and physiological function (Wess, 2003). Defining the contribution of individual classes of cholinergic modulatory interneurons to specific behaviors has therefore been a challenge.

The spinal cord contains several classes of cholinergic interneurons with proposed roles in sensory processing and motor output (Barber et al., 1984; Phelps et al., 1984; Huang et al., 2000). The best-characterized spinal cholinergic circuit involves a recurrent excitatory connection from motor neurons to Renshaw interneurons, mediated by the activation of nicotinic receptors (Willis, 1971; Alvarez and Fyffe, 2007). Motor neurons themselves also receive synaptic input from recurrent motor axon collaterals (Lagerbäck et al., 1981). But the most prominent cholinergic input to motor neurons takes the form of C boutons, a set of large synaptic terminals that are concentrated on motor neuron cell bodies and proximal dendrites (Conradi and Skoglund, 1969; Nagy et al., 1993; Li et al., 1995). Cholinergic C boutons align with postsynaptic m2 class muscarinic receptors and Kv2.1 class K^+ channels (Hellström et al., 2003; Muennich and Fyffe, 2004; Wilson et al., 2004), suggesting that these synapses exert a modulatory influence on motor neuron firing (Brownstone et al., 1992). The activation of muscarinic receptors

on spinal neurons reduces spike afterhyperpolarization and leads to a marked enhancement in the frequency of motor neuron firing (Miles et al., 2007). Conversely, blockade of muscarinic receptors in isolated spinal cord preparations decreases motor neuron output (Miles et al., 2007). Together, these findings have led to the idea that C bouton synapses exert a modulatory influence on spinal motor output.

The neuronal source of C bouton terminals has proved elusive. They do not derive from descending supraspinal axons (McLaughlin, 1972; VanderHorst and Ulfhake, 2006) or from motor axon collaterals (Hellström et al., 1999; Miles et al., 2007), and so by elimination are thought to originate from one or more populations of spinal interneurons. The persistence of C boutons after intraspinal lesions has led to the suggestion that they derive from cholinergic interneurons that are interspersed among motor neurons in the ventrolateral spinal cord (Hellström, 2004). Analysis of the activity-induced pattern of c-*fos* expression during locomotion, however, shows strong labeling of cholinergic interneurons adjacent to the central canal (Huang et al., 2000). Consistent with this, genetic lineage tracing in mice has provided evidence that C boutons derive from one or more of the cholinergic interneuron classes that populate the intermediate zone of the spinal cord (Miles et al., 2007). But since there are no selective molecular markers for neurons that give rise to C boutons, the circuitry and physiology of this intrinsic cholinergic system, and its contribution to mammalian motor behavior, have yet to be defined.

We set out to define discrete functional populations of interneurons in mouse spinal cord on the basis of their transcription factor profile, neurotransmitter phenotype, and connectivity. We show here that the paired-like homeodomain transcription factor Pitx2 (Semina et al., 1996) defines a small set of cholinergic V0 interneurons positioned close to the central canal, and we establish that these neurons represent the sole source of C bouton synapses. The firing of cholinergic V0 interneurons is tightly phase locked with motor neuron burst activity during fictive locomotor episodes, indicative of their recruitment during motor behavior. To explore the consequences of inactivating the output of these cholinergic interneurons, we eliminated choline acetyl transferase (ChAT), the sole synthetic enzyme for acetylcholine (ACh), from cholinergic V0 neurons. Mice in which cholinergic V0 neurons have been deprived of ChAT expression are impaired in their ability to increase the activation of specific muscles during certain locomotor behaviors, suggesting that recruitment of this set of cholinergic interneurons is required for the task-dependent enhancement of motor neuron firing. Together, our findings define the organization and properties of a discrete set of spinal cholinergic interneurons that exert a context-dependent modulatory influence on motor behavior.

RESULTS

Pitx2 Is Expressed by a Small Subset of V0 Interneurons

To define markers of discrete sets of spinal interneurons, we performed a microarray screen with cDNA probes derived from dorsal and ventral domains of p8 mouse lumbar spinal cord (Figure S1A). We identified 82 genes with a ventral:dorsal enrichment ratio of 3.0 or greater and used in situ hybridization histochemistry to determine the profile of expression of these genes. This analysis identified seven genes with patterns of expression that were confined to subsets of interneurons in intermediate and ventral spinal cord (Figure S1B–S1F). In this study, we focus on the phenotype, organization, and function of interneurons defined by one of these genes, which encodes the paired-like homeodomain protein Pitx2 (Semina et al., 1996).

In postnatal lumbar spinal cord, expression of *Pitx2* was confined to a longitudinally arrayed cluster of cells positioned close to the central canal (Figures 1A and 1B). A similar profile of *Pitx2* expression was detected at thoracic and cervical levels, although at cervical levels the domain of *Pitx2*$^+$ neurons extended slightly more laterally (Figures 1C and 1D). From the outset, *Pitx2* expression was restricted to a small group of neurons (Figures S2A–S2C). At lumbar levels, *Pitx2* expression was first detected at embryonic day (e) 11.5 to 12.0 (Figure S2C) and, by late embryonic stages, was restricted to a small group of neurons in the intermediate domain, close to the central canal (Figure S2D). The expression of *Pitx2* by neurons in this medial column persisted until at least p30 (Figure S2E).

Pitx2$^+$ neurons comprised two phenotypic subsets: one that coexpressed the cholinergic markers ChAT and vAChT (vesicular acetylcholine transporter) and a second that expressed the vesicular glutamate transporter *vGluT2* (Figures 1E–1I″). Neurons in the pericentral canal region of p8 lumbar spinal cord did not coexpress *vAChT* and *vGluT2* (Figure S3), indicating that these two neurotransmitter-defined sets represent distinct subpopulations. Cholinergic and glutamatergic Pitx2$^+$ neurons were differentially distributed along the rostro-caudal axis of the lumbar spinal cord. At rostral lumbar levels, the majority of Pitx2$^+$ neurons expressed cholinergic markers, whereas glutamatergic Pitx2$^+$ neurons predominated at more caudal lumbar levels (Figure 1J). Cholinergic and glutamatergic Pitx2$^+$ neurons were also detected at thoracic and cervical levels of the spinal cord (data not shown). Thus, Pitx2 marks a small subset of interneurons that can be further subdivided on the basis of neurotransmitter phenotype. Pitx2 expression distinguishes this set of cholinergic interneurons from a nearby population of central canal cluster (C^3) neurons (Barber et al., 1984; Phelps et al., 1984) that also express cholinergic phenotype, but lack Pitx2 expression (Figure S4).

We used genetic lineage tracing to determine the developmental origin of cholinergic and glutamatergic Pitx2$^+$ neurons. The provenance of these interneurons was analyzed in a *Dbx1::nlsLacZ* transgenic line in which the postmitotic perdurance of LacZ expression marks V0 interneurons (Pierani et al., 2001). In e12.5 *Dbx1::nlsLacZ* mice, we found that ~80% of Pitx2$^+$ neurons coexpressed LacZ (Figures 1L–M′), indicating that they correspond to V0 neurons. Analysis of *Dbx1* null mutant embryos, which lack V0 interneurons (Pierani et al., 2001), revealed an absence of Pitx2 expression from neurons in the intermediate spinal cord (Figures 1N and 1O), confirming the V0 identity of Pitx2$^+$ interneurons. This transcriptionally defined population represents a very minor subset of the total V0 interneuron cohort: Pitx2 was expressed by only 5% of all LacZ$^+$ neurons in e12.5 *Dbx1::nlsLacZ* embryos (Figures 1K and 1L). V0 interneurons have been shown to comprise Evx1/2$^+$ ($V0_V$)

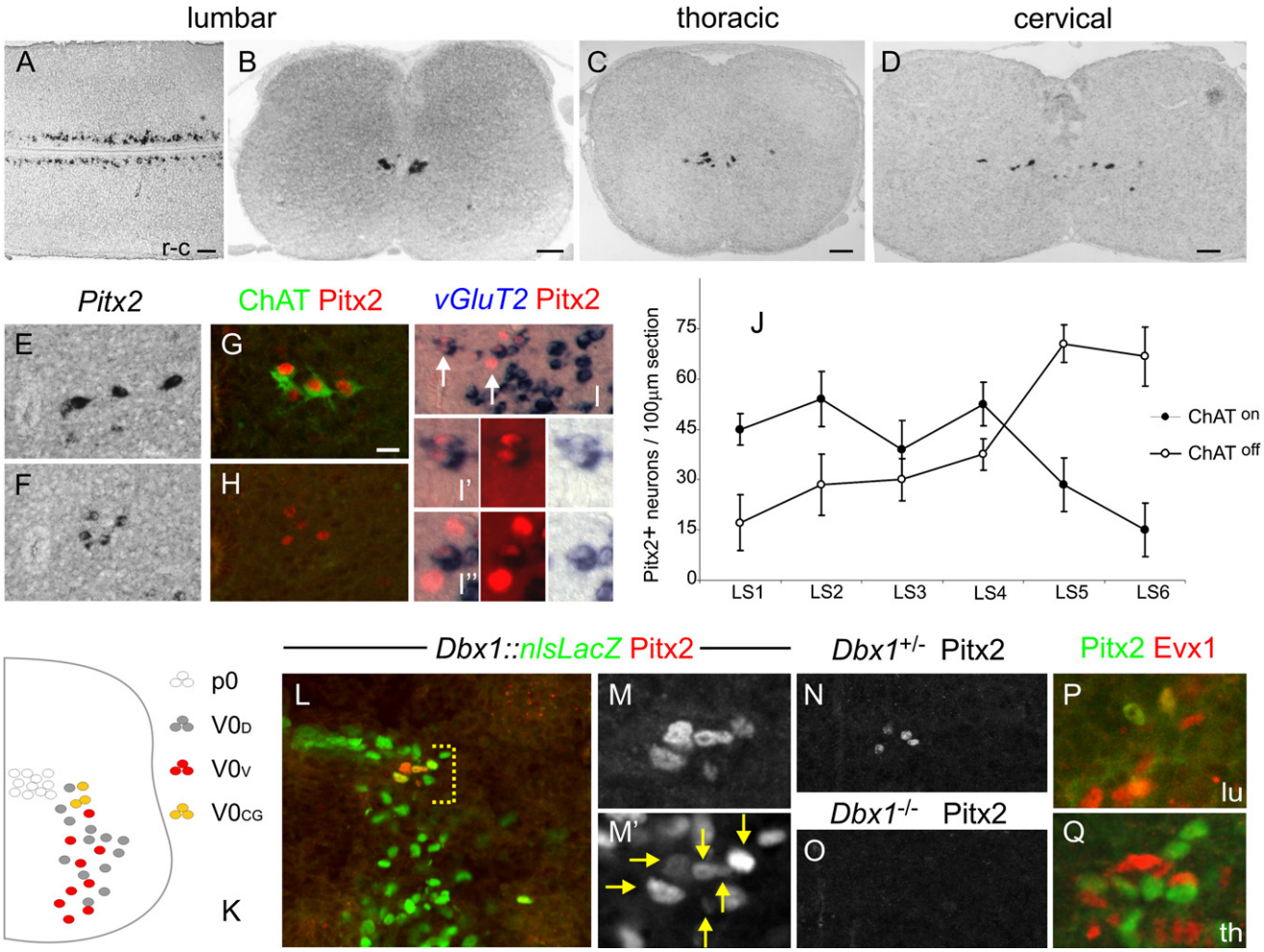

Figure 1. Origin and Neurotransmitter Phenotype of Spinal Pitx2$^+$ Neurons

(A–D) *Pitx2* expression in e17.5 (A) and p8 (B–D) spinal cord. Spinal *Pitx2* (*munc-30*) expression has been noted (Nicholson et al., 2001).

(E–J) Neurotransmitter phenotype of Pitx2$^+$ neurons in p8 spinal cord. *Pitx2* expression in rostral (E) and caudal (F) lumbar levels. ChAT and Pitx2 expression in rostral (G) and caudal (H) lumbar levels. (I–I″) vGluT2 expression in a subset of lumbar Pitx2$^+$ neurons. Arrows in (I) indicate cells shown in higher magnification in (I′) and (I″). (J) Cholinergic Pitx2$^+$ neurons predominate at upper lumbar levels, whereas at lower lumbar levels most Pitx2$^+$ neurons are glutamatergic. Data from three p4 and two p8 mice (mean ± SE) per 100 μm. Greater than 90% of all Pitx2$^+$ neurons can be accounted for by ChAT or vGluT2 expression.

(K) Origin and diversity of p0 domain-derived V0 neurons. For details, see text and Lanuza et al. (2004).

(L–Q) Pitx2$^+$ neurons derive from p0 domain progenitors. Most Pitx2$^+$ neurons express nuclear LacZ in a *Dbx1::LacZ* transgene in e12.5 spinal cord (L, M, and M′). Arrows indicate double-labeled cells. Pitx2 is expressed in e16.5 *Dbx1* heterozygous mice (N) but expression is lost in *Dbx1* mutant mice (O). (P) Evx1 expression at lumbar (lu) levels and (Q) thoracic (th) levels at e12.5. Virtually all newly generated Pitx2$^+$ neurons coexpress Evx1, but by e14, Evx1 expression has been extinguished from most neurons. In addition to the Pitx2$^+$ V0 population, rare Pitx2$^+$ neurons are detected in the dorsal spinal cord (1.6 neurons/100 μm; n = 6 mice) (Figure S7). These noncholinergic neurons could correspond to neurons described by Polgár et al. (2007).

Scale bars = 100 μm (A–D), 20 μm (G).

and Evx1/2$^-$ (V0$_D$) divisions (Lanuza et al., 2004). Soon after their generation, virtually all Pitx2$^+$ neurons coexpressed Evx1, albeit transiently (Figures 1P and 1Q). Thus, the cholinergic (V0$_C$) and glutamatergic (V0$_G$) interneuron populations marked by Pitx2 appear to constitute small subsets of V0$_V$ interneurons.

Genetic Tracing of V0$_C$ and V0$_G$ Interneuron Connectivity

To define the connectivity of V0$_C$ and V0$_G$ neurons, we crossed a mouse *Pitx2::Cre* line, which directs expression of Cre recombinase selectively in Pitx2$^+$ neurons (Liu et al., 2003) with conditional *Thy1.lsl.YFP* or *Tau.lsl.mGFP* reporter strains (Buffelli et al., 2003; Bareyre et al., 2005; Hippenmeyer et al., 2005). We detected fluorescent protein (FP) expression in a small subset of interneurons close to the central canal (Figures 2A and 2B). At rostral lumbar levels, FP expression was detected in 66% of all Pitx2$^+$ neurons in *Thy1.lsl.YFP* mice and in 74% of all Pitx2$^+$ neurons in *Tau.lsl.mGFP* mice (Figures 2C–2D′ and data not shown). Examination of the neurotransmitter status of genetically marked neurons in *Tau.lsl.mGFP* mice revealed FP expression

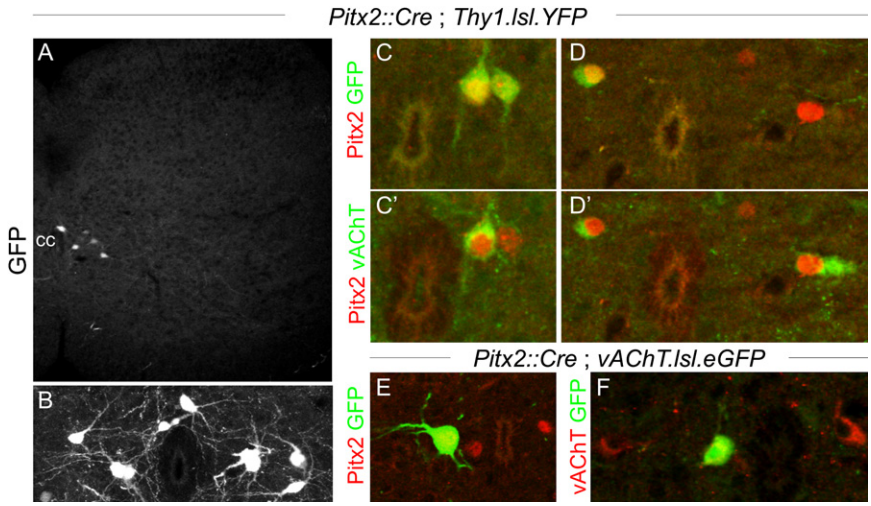

Figure 2. Genetic Marking of Pitx2$^+$ Neurons

(A–D′) Genetic marking of Pitx2$^+$ neurons in *Pitx2::Cre*;*Thy1.lsl.YFP* mice.

(A and B) Fluorescent protein (FP) is expressed in a small subset of pericentral canal neurons (central canal [cc]). (B) shows high-power view of the pericentral canal region.

(C and D) In this *Thy1* line, FP is expressed in 66% of Pitx2$^+$ neurons. (C′ and D′) Pitx2 and vAChT expression at rostral lumbar levels.

(E and F) Genetic marking of V0$_C$ neurons in *Pitx2::Cre*;*vAChT.lsl.eGFP* mice reveals FP expression in Pitx2$^+$ and vAChT$^+$ neurons.

in 94% of cholinergic Pitx2$^+$ interneurons and in 56% of noncholinergic Pitx2$^+$ interneurons. Thus, V0$_C$ interneurons are labeled with high efficiency in *Tau.lsl.mGFP* mice.

To trace the targets of V0$_C$ and V0$_G$ neurons, we mapped FP-labeled axons and terminals in the spinal cord of *Pitx2::Cre*;*Tau.lsl.mGFP* mice, in conjunction with synaptic expression of the cholinergic markers vAChT and ChAT, and the glutamatergic marker vGluT2. Analysis of the overall pattern of FP-labeled axons and terminals from p8 to p25 revealed a high density in the ventral horn and intermediate zone and a lower density in the dorsal horn (Figures 3A and S5). In the ventral horn, the cell bodies and proximal dendrites of virtually all vAChT$^+$ motor neurons were studded with large FP-labeled boutons (Figures 3B and 3C), whereas more distal dendritic domains exhibited a >20-fold lower FP$^+$ bouton density (Figures 3H and 3I). We found that ~99% of the FP-labeled boutons on motor neurons expressed vAChT, and none of them coexpressed vGluT2 (Figures 3D–3D‴). Conversely, 95% of all vAChT$^+$ C boutons on motor neurons expressed FP. Consistent with their identity as C boutons, FP-labeled terminals on motor neurons were aligned with postsynaptic m2 muscarinic receptors and Kv2.1 channels (Figures 3F and 3G). These findings, taken together with the 94% labeling efficiency of cholinergic Pitx2$^+$ interneuron cell bodies, indicate that V0$_C$ neurons represent the sole source of C boutons. Moreover, motor neurons receive preferential input from the V0$_C$ subset of Pitx2$^+$ neurons.

We next examined the connectivity of Pitx2$^+$ neurons with spinal interneurons. We detected FP-labeled vGluT2$^+$ boutons in the intermediate zone and dorsal horn of *Pitx2::Cre*;FP reporter mice (Figures 3E–3E″; data not shown), providing evidence that the V0$_G$ class of Pitx2$^+$ neurons forms connections with spinal interneurons. We also detected a low density of FP-labeled vAChT$^+$ boutons in the intermediate zone of the spinal cord of p20– p40 *Pitx2::Cre*;*Tau.lsl.mGFP* mice (data not shown), suggestive of synaptic contact with ventral interneurons. We therefore examined whether two classes of interneurons implicated in the regulation of motor neuron output, V2a interneurons (Peng et al., 2007; Al-Mosawie et al., 2007; Lundfald et al., 2007; Crone et al., 2008) and Renshaw cells (Alvarez and Fyffe, 2007), are contacted by V0$_C$ neurons. The cell bodies and proximal dendrites of V2a neurons, defined by FP expression in *Sox14::eGFP* mice (Crone et al., 2008), were contacted only sparsely by vAChT$^+$ boutons (<4 boutons/neuron; 37 neurons) but by many vGluT1$^+$ terminals (Figures 4A–4D″ and 4R; Al-Mosawie et al., 2007). The cell bodies and dendrites of calbindin$^+$ Renshaw cells were contacted by many vAChT$^+$ boutons (Figures 4A, 4E, 4F, and 4R). But analysis of *Pitx2::Cre*;*Tau* or *Thy1* reporter mice revealed that none of them were FP labeled (Figures 4E and 4F, 0/132 boutons; 8 neurons). Thus, Renshaw cells lack V0$_C$ (or V0$_G$) input, although they receive cholinergic innervation from the axon collaterals of motor neurons (Figures 4G and 4H–4H″). These findings argue for selectivity in the target connectivity of V0$_C$ interneurons (Figure 4R). To assess whether Pitx2$^+$ V0 neurons innervate ipsilateral and/or contralateral targets, we identified interneurons after unilateral hindlimb muscle injection of pseudorabies PRV 614 (mRFP1) transneuronal tracer in p15 and p30 mice (Banfield et al., 2003; Smith et al., 2000; Lanuza et al., 2004). 48–68 hr after virus injection, 69% of GFP-labeled Pitx2$^+$ neurons were located ipsilateral to the side of muscle injection, (54/78 labeled neurons; Figure S6), indicating that many Pitx2$^+$ V0 neurons project to ipsilateral motor neurons.

We also assessed the nature and origin of synaptic inputs to V0$_C$ interneurons. In p24 *Pitx2::Cre*;*Thy1.lsl.YFP* mice, the cell bodies of vAChT$^+$, FP-labeled V0$_C$ neurons received many vGluT2$^+$ bouton contacts (>50 per neuron), an indication of excitatory input from glutamatergic interneurons and/or descending projections (Figures 4I–4L). In contrast, we detected few vGluT1$^+$ synaptic contacts (~10 boutons per neuron; Figures 4P–4P‴), reflecting sparse sensory and/or corticospinal input (Betley et al., 2009). vAChT$^+$, FP-labeled V0$_C$ neurons also received many GAD67$^+$ GABAergic inhibitory inputs (>50 boutons per neuron) (Figures 4Q–4Q‴). We also detected serotonergic contacts (>20 per neuron) on the cell body and proximal dendrites of FP-labeled V0$_C$ neurons (Figures 4M–4O and 4R), presumably reflecting brainstem serotonergic input. Thus, V0$_C$ neurons receive input from glutamatergic, GABAergic, and monoaminergic pathways.

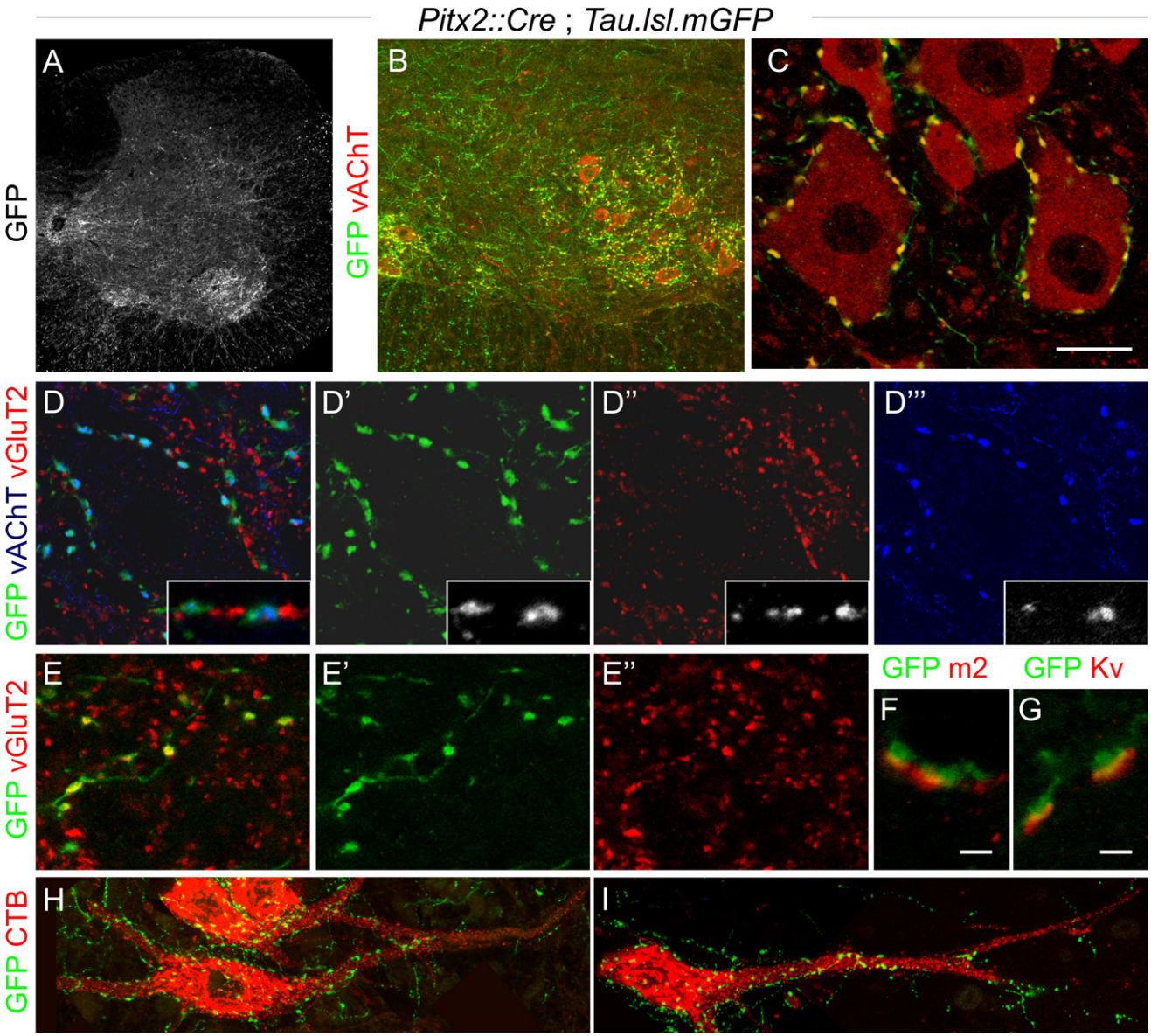

Figure 3. Genetic Tracing of $V0_C$ Neuronal Connections with Motor Neurons

(A) Spatial distribution of $V0_C$ and $V0_G$ axons and terminals in lumbar spinal cord of *Pitx2::Cre*;*Tau.lsl.mGFP* reporter mice.

(B and C) Coexpression of FP and vAChT in C boutons. Greater than 95% of $vAChT^+$ terminals on motor neurons express FP. The density of FP-labeled boutons on motor neurons that innervate proximal hindlimb muscles was ~3-fold greater than that on motor neurons innervating distal footpad (plantar) muscles, consistent with the known pattern of C bouton innervation (Hellström, 2004).

(D–D″′) FP^+ terminals motor neurons express vAChT but not vGluT2.

(E–E″) FP^+ terminals in the intermediate spinal cord express vGluT2.

(F and G) In *Pitx2::Cre*;*Tau.lsl.mGFP* mice, m2 muscarinic receptor (m2) and Kv2.1 channel (Kv) clusters are aligned with FP^+ C boutons.

(H and I) FP^+ C boutons are concentrated on motor neuron somata and proximal dendrites. Cholera toxin B (CTB) subunit-labeled tibialis anterior motor neurons in lumbar spinal cord of a p24 *Pitx2::Cre*;*Tau.lsl.mGFP* mouse. FP-labeled terminals are detected on the soma and proximal dendrites (15.7 C boutons/50 μm length of proximal dendrite, n = 3), but more distal dendritic domains are devoid of FP^+ terminals.

Scale bars = 20 μm (C), 2 μm (F and G).

Coordination of $V0_C$ Neuron and Motor Neuron Activity during Locomotor Episodes

We examined the physiological properties and functional connectivity of $Pitx2^+$ V0 neurons using whole-cell patch-clamp recordings from FP-labeled neurons in hemisected lumbar spinal cord preparations obtained from p4 to p8 *Pitx2::Cre*;*Thy1.lsl.YFP* mice (Figures 5A–5D). FP-labeled neurons exhibited low whole-cell capacitance and moderate input resistance

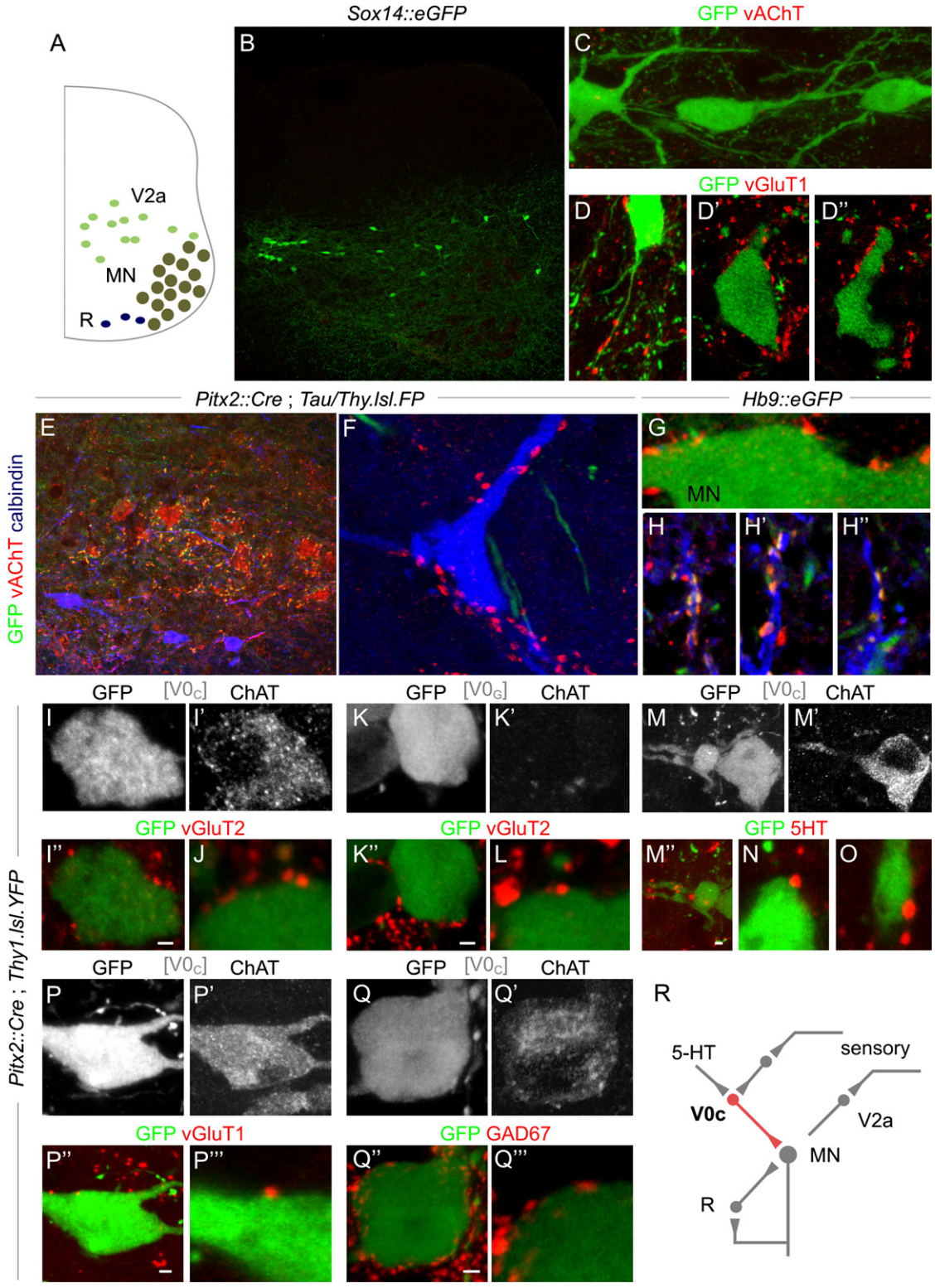

Figure 4. The Synaptic Circuitry of $V0_C$ Interneurons

(A–H″) Lack of connectivity of $V0_C$ neurons with identified interneurons.

(A) Motor neuron (MN), $Sox14^+$ V2a interneuron (V2a), and $calbindin^+$ Renshaw cell (R) position in lumbar spinal cord.

(B) GFP^+ V2a interneurons in lumbar spinal cord of p15 *Sox14::eGFP* mice.

(~30 pF, ~450 MΩ, 16 neurons in control solution). At rest, 63% of FP-labeled neurons exhibited spontaneous activity, at low mean firing rates (3.1 ± 0.5 Hz, 10/16 neurons), with long action potentials (half-width = 2.81 ± 0.2 ms), and a prominent afterhyperpolarization (Figure 5E). Intracellular current injection enhanced firing rates to ~20 Hz, with little spike frequency adaptation (Figures 5F–5H; 16 neurons). These features varied little among FP-labeled neurons, implying that $V0_C$ and $V0_G$ neurons share similar biophysical properties.

We next analyzed Pitx2$^+$ V0 neuron firing frequency with motor neuron bursting during fictive locomotor activity. Whole-cell patch-clamp recordings were obtained from FP-labeled neurons at rostral lumbar levels in hemisected spinal cord preparations exposed to a rhythmogenic drug cocktail (Figures 6A–6C; Jiang et al., 1999). Most FP-labeled neurons (14/16 neurons) were tonically active (Figure 6A), and a few exhibited marked bursting activity (Figure 6C). The firing rate of tonically active FP-labeled neurons was modulated: ~80% of neurons fired more rapidly in phase with motor burst activity in flexor associated L1–L3 ventral roots (Figure 6A; ~1.5-fold > firing rate, $p < 0.01$ for 9/11 FP-labeled neurons). This phasic relationship was revealed most clearly when FP-labeled V0 neurons were hyperpolarized by current injection (−10 pA to −100 pA; Figure 6B). Under these conditions, ~90% of all FP-labeled neurons at L1 to L3 segments were phase locked with motor neuron bursts recorded from flexor-associated L1–L3 ventral roots (Figures 6E and 6F, closed circles, 14/16 neurons). On occasion, rostrally positioned V0 neurons also exhibited isolated interburst spikes (Figure 6C). Strikingly, these spikes coincided with transient excitatory activity recorded from L1–L3 ventral roots, as well as with brief periods of motor inactivity recorded from L5 motor roots (Figure 6C, arrows). At L4 to L5 segments, some FP-labeled V0 neurons fired maximally in phase with extensor-associated L4–L5 ventral root bursts (three neurons), although others fired in phase with L1–L3 ventral root bursts (three neurons; Figure 6F, open circles). The activity of Pitx2$^+$ V0 neurons is therefore linked predominantly to the output of their segmentally aligned motor neuron targets, exclusively so at rostral lumbar levels.

Most Pitx2$^+$ interneurons at rostral lumbar levels are cholinergic, suggesting that the phasic features of the general population of FP-labeled Pitx2$^+$ V0 neurons are representative of the behavior of $V0_C$ neurons. To define the properties of identified $V0_C$ neurons, we analyzed mice in which $V0_C$ neurons are marked selectively by crossing the *Pitx2::Cre* line with a *vAChT* FP reporter line (Figures 2E and 2F) (Experimental Procedures). At rostral lumbar levels, identified *vAChT* FP-labeled $V0_C$ neurons also exhibited tonic activity with maximal firing in register with L1–L3 ventral root motor bursts (Figures 6D and 6F, open triangles, four neurons). The coordinated firing of Pitx2$^+$ excitatory V0 neurons and motor neurons raises the possibility that these interneurons regulate ipsilateral motor output during locomotor activity.

To explore the basis of the phasic activity of Pitx2$^+$ V0 interneurons, we first assessed whether these neurons display intrinsic oscillatory properties. Whole-cell patch-clamp recordings were made from FP-labeled neurons in transverse spinal cord slices obtained from p12–p13 *Pitx2::Cre*;*Tau.lsl.mGFP* mice. FP-labeled neurons were spontaneously active and the application of a rhythmogenic drug cocktail increased the firing rate of FP-labeled neurons, but oscillatory activity was not observed (Figures 5I and 5J; six neurons), suggesting that they lack intrinsic rhythmogenic properties.

To assess the origin of inputs responsible for the phasic activity of Pitx2$^+$ V0 interneurons, we recorded from FP-labeled neurons in L1–L3 segments in hemisected spinal preparations. Antidromic activation of motor neurons by ventral root stimulation did not elicit synaptic responses in FP-labeled V0 neurons (four neurons; data not shown), arguing against input from a recurrent excitatory pathway (Machacek and Hochman, 2006). Voltage-clamp analysis of FP-labeled neurons during locomotor activity revealed barrages of excitatory postsynaptic current (EPSCs) in phase with ventral root bursts (Figures 7A and 7B; 13 *Thy1* FP-labeled neurons; four *vAChT* FP-labeled neurons). In contrast, IPSCs were detected during all phases of the motor burst cycle (Figures 7C, seven *Thy1* FP-labeled neurons). Together, these findings support the idea that the bursting activity of Pitx2$^+$ V0 neurons is driven by rhythmic excitatory input from spinal interneurons.

We also asked whether Pitx2$^+$ V0 interneurons can be activated by sensory afferent input. Recordings from FP-labeled neurons during stimulation of segmentally aligned dorsal roots (threshold 10–40 μA) revealed sensory-evoked EPSCs (Figure 7D). Their latency (14.1 ± 1.0 ms, seven *Thy1* FP-labeled neurons), variable onset (high "jitter," coefficient of variation = 0.18) is indicative of indirect rather than monosynaptic excitatory input. Together, these physiological studies in isolated spinal cord preparations indicate that the phasic activity of Pitx2$^+$ V0 interneurons is driven primarily by input from local excitatory interneurons.

(C) GFP-labeled Sox14$^+$ neurons are contacted by few vAChT$^+$ terminals (<4 boutons per neuron, 37 neurons).
(D–D″) vGluT1$^+$ terminals on dorsally located Sox14$^+$ interneurons.
(E and F) In p24 *Pitx2cre*;*Tau*/*Thy1.lsl.FP* mice, calbindin$^+$ Renshaw cells are contacted by vAChT terminals that do not express FP (n = 0/132 boutons, 8 neurons).
(G) GFP$^+$ motor neurons in *Hb9::eGFP* mice lack FP$^+$ vAChT input.
(H–H″) In p21 *Hb9::eGFP* mice, most vAChT$^+$ terminals on calbindin$^+$ Renshaw cells express FP.
(I–Q‴) Synaptic inputs to p24 $V0_{CG}$ interneurons.
(I and J) ChAT$^+$, GFP$^+$ $V0_C$ neurons contacted by vGluT2$^+$ boutons. Panel (J) shows a different neuron.
(K and L) ChAT^{off}, GFP$^+$ $V0_G$ neurons also contacted by vGluT2$^+$ boutons. Panel (L) shows a different neuron.
(M–O) ChAT$^+$, GFP$^+$ $V0_C$ neurons contacted by 5HT$^+$ boutons. Panels (N) and (O) show different neurons.
(P–P‴) ChAT$^+$, GFP$^+$ $V0_C$ neurons contacted by vGluT1$^+$ boutons.
(Q–Q‴) ChAT$^+$, GFP$^+$ $V0_C$ neurons contacted by GAD67$^+$ boutons.
(R) Connectivity of $V0_C$ neurons.
Scale bar = 2 μm (I″, K″, M″, P″, and Q″).

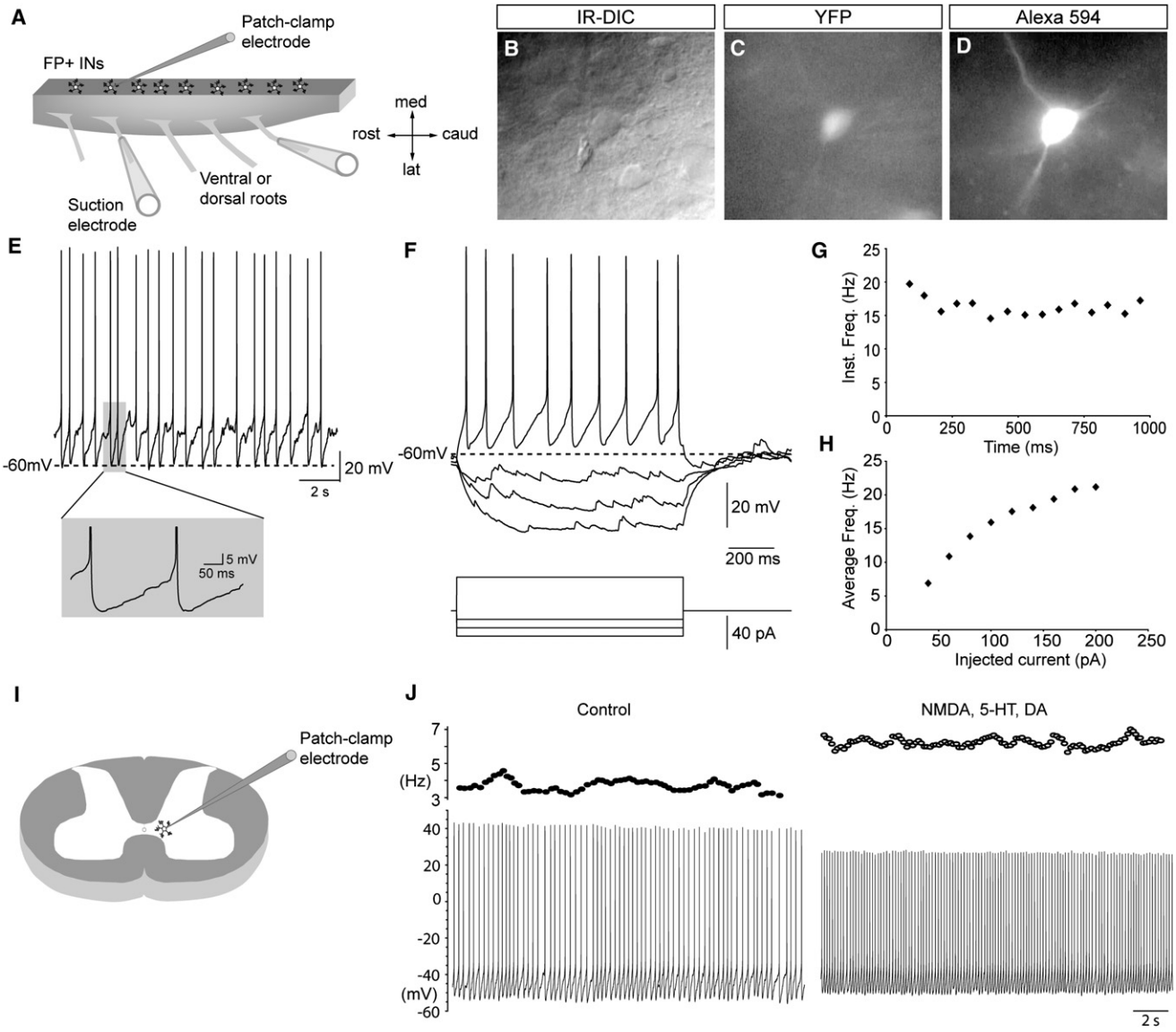

Figure 5. Intrinsic Properties of Pitx2^{+} V0$_{CG}$ Interneurons

(A) Hemisected spinal cord preparation used for physiology.

(B–D) IR-DIC and fluorescence images of an identified V0$_{CG}$ neuron from a *Pitx2::Cre*;*Thy1.lsl.YFP* mouse. The cell was patch clamped under IR-DIC optics and filled with Alexa 594 during recording.

(E) Slow-frequency, tonic activity recorded from an FP-labeled V0$_{CG}$ neuron. Prominent afterhyperpolarization shown in gray inset.

(F) Recordings from an FP-labeled V0$_{CG}$ neuron after injection of depolarizing and hyperpolarizing current pulses (1 s duration). Bottom trace shows injected current.

(G) Instantaneous firing frequency of an FP-labeled V0$_{CG}$ neuron in response to 1 s injection of depolarizing current.

(H) Steady-state firing frequency—current plot (*f-I*) for an FP-labeled V0$_{CG}$ neuron upon injection of incremental (1 s) depolarizing current steps.

(I) Spinal cord slice preparation.

(J) Instantaneous firing frequency (moving average of five consecutive spikes; top) and corresponding current-clamp recordings (bottom) from a tonically active *Thy1* FP-labeled V0$_{CG}$ neuron in a slice preparation. Control (left) and with NMDA (5 μM), 5-HT (10 μM), and dopamine (50 μM) (right).

A Motor Behavioral Defect in Mice Lacking V0$_{C}$ Cholinergic Output

To explore the contribution of V0$_{C}$ interneurons to locomotor behavior, we sought a means of inactivating the output of this set of neurons while preserving the function of other classes of V0 neurons. Cre-mediated deletion of coding exons of the mouse *ChAT* gene generates a truncated, enzymatically inactive protein and effectively prevents cholinergic transmission by

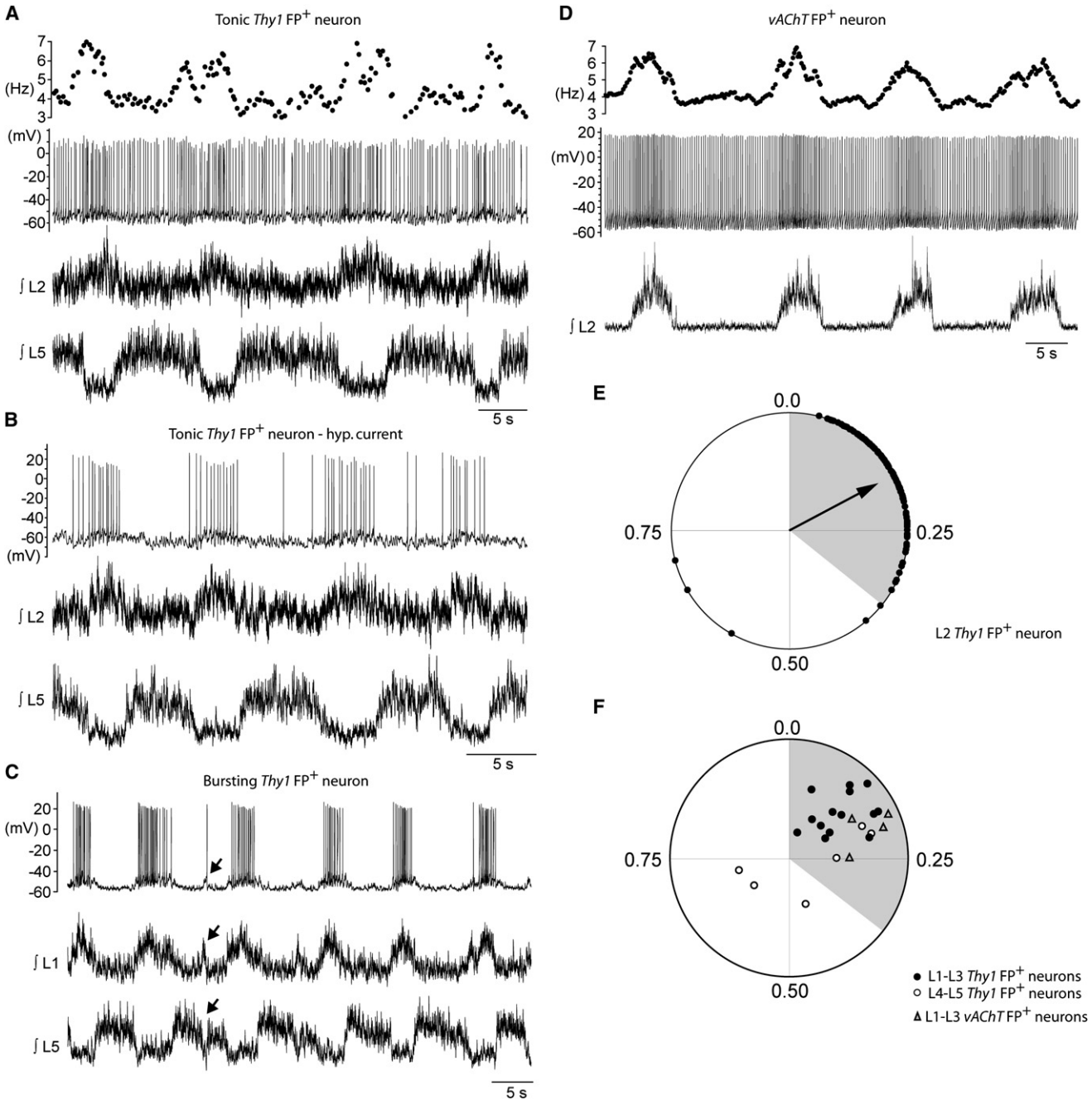

Figure 6. Activity of Pitx2$^+$ V0$_{CG}$ Neurons during Locomotor Episodes

(A) Moving average (five consecutive spikes) of the instantaneous firing frequency of a tonically active *Thy1* FP-labeled V0$_{CG}$ neuron (top trace) along with the corresponding current-clamp recording (second trace) and rectified/integrated ventral root recordings (bottom traces) during drug-induced (NMDA 5 μM, 5-HT 10 μM, dopamine 50 μM) locomotor activity in a hemisected spinal cord preparation.

(B) Phasic activity recorded from neuron in (A) during the injection of hyperpolarizing current (top trace) along with rectified/integrated recordings of locomotor activity from ventral roots (bottom traces).

(C) Recording from a bursting *Thy1* FP-labeled V0$_{CG}$ neuron (top trace) and rectified/integrated recordings of locomotor activity from ventral roots (bottom traces). The coupling between the spiking of this FP-labeled V0$_{CG}$ neuron and ventral root activity is indicated by arrows.

(D) Moving average (five consecutive spikes) of the instantaneous firing frequency of a tonically active *vAChT* FP-labeled V0$_C$ neuron (top trace) along with the corresponding current-clamp recording (second trace) and rectified/integrated recordings of locomotor activity from ventral roots (bottom traces).

(E) Circular plot for the FP-labeled V0$_{CG}$ neuron shown in *C* depicting its preferred firing phase (mean vector; arrow) in relation to the locomotor cycle. The start of the locomotor cycle (0.0) is taken as the onset of the burst in the rostral lumbar ventral root. Shaded area highlights the average duration of rostral lumbar root

spinal neurons (Misgeld et al., 2002; Buffelli et al., 2003). We used this strategy to generate a V0 neuron-specific disruption in the gene encoding ChAT.

We compared the efficacy of ChAT elimination from $V0_C$ neurons in mice in which *Pitx2::Cre* and *Dbx1::Cre* (Bielle et al., 2005) driver lines were crossed with a floxed *ChAT* (*ChAT^{fl}*) allele (Buffelli et al., 2003). In *Pitx2::Cre*;*ChAT$^{fl/fl}$* mice analyzed between p0 and p30, ChAT expression was eliminated from ~55% of vAChT$^+$ C boutons (data not shown). In contrast, *Dbx1::Cre*;*ChAT$^{fl/fl}$* mice exhibited a virtually complete (>99%, n = 503 boutons) loss of vAChT$^+$, ChAT$^+$ C boutons (Figures 8A–8F″). The depletion of ChAT in *Dbx1::Cre*;*ChAT$^{fl/fl}$* mice was selective, in that motor neurons still expressed ChAT (Figures 8A and 8D). C^3 neurons can be labeled by *Dbx1::*Cre lineage tracing (Miles et al., 2007) (Figure S4), but C bouton synapses with motor neurons derive exclusively from $V0_C$ neurons. Moreover, the axonal projections of C^3 neurons appear confined to the vicinity of the central canal (Barber et al., 1984; Phelps et al., 1984). Thus, the connectivity of C^3 neurons excludes a direct influence on motor output. We therefore analyzed the impact of eliminating $V0_C$ output on locomotor behavior using *Dbx1::Cre*;*ChAT$^{fl/fl}$* mice.

Dbx1::cre;*ChAT$^{fl/fl}$* mice exhibited an overtly normal developmental program and survived until adulthood (data not shown). Despite the loss of synaptic ChAT expression, the number of vAChT$^+$ C boutons in contact with the cell body and proximal dendrites of lumbar motor neurons was similar in *Dbx1::Cre*;*ChAT$^{fl/fl}$*, *Dbx1::Cre*;*ChAT$^{fl/+}$*, and wild-type mice (Figures 8A and 8D; data not shown). The loss of ChAT expression from C boutons was not accompanied by expression of the glutamatergic markers vGluT1 or vGluT2 (Figures 8G–8H″). These vAChT$^+$, ChAT-depleted C boutons were still aligned with m2 muscarinic receptors and Kv2.1 class K$^+$ channels (Figures 8I–8J″), indicating that the postsynaptic organization of these synapses is preserved. Thus, ChAT-deficient $V0_C$ neurons form structurally differentiated, albeit acetylcholine-synthesis-deficient, synapses with motor neurons.

To examine the contribution of $V0_C$ neurons to motor output, we focused on locomotor behavioral assays that uncover task-dependent modulation in the activation of limb muscles. In rodents, walking and swimming elicit markedly different degrees of hindlimb muscle activation (Roy et al., 1985; de Leon et al., 1994)—the amplitude of gastrocnemius (Gs) electromyographic (EMG) activity, for instance, is greater during swimming than walking (Hutchison et al., 1989). We therefore monitored the degree of Gs muscle activation in mice subjected sequentially to walking and swimming.

To measure muscle activation, the Gs muscles of wild-type (n = 8), *ChAT$^{fl/fl}$* (n = 14), and *Dbx1::Cre*;*ChAT$^{fl/fl}$* (n = 12) mice (p45 or older) were implanted with EMG recording electrodes (Pearson et al., 2005; Akay et al., 2006). Electrodes were also placed in the left and right tibialis anterior (TA) ankle flexor and Iliopsoas (Ip) hip flexor muscles as indicators of the overall fidelity of locomotor pattern. We detected no consistent differences in EMG patterns of control and *Dbx1::Cre*;*ChAT$^{fl/fl}$* mice during locomotor behavior. A clear alternation of Gs, compared to TA and Ip muscle activity, was evident during walking (Figures 9A and 9B). The normal alternation in the activity of left and right TA muscles was also preserved in *Dbx1::Cre*;*ChAT$^{fl/fl}$* mutant mice (Figures 9A and 9B). Thus, loss of $V0_C$ neuronal output does not perturb locomotor pattern.

We next examined muscle activity in wild-type mice during walking and swimming. The amplitude of the Gs muscle burst in control mice subjected to a swimming task was consistently larger than the burst observed when the same animals were walking (Figure 10A). The amplitude of TA muscle bursts was only marginally greater during swimming than walking, however (Figure 10A). We quantified the change in muscle activity during swimming and walking by monitoring the ratio of peak swim:walk (S:W) EMG amplitudes, revealing S:W ratios of 5.5 for the Gs muscle and 1.3 for the TA muscle (Figures 10B and 10D).

In *Dbx1::Cre*;*ChAT$^{fl/fl}$* mice subjected sequentially to walking and swimming tasks, we observed that the enhancement of Gs burst amplitude during swimming was significantly diminished (S:W ratio of 3.5, $p < 0.01$) (Figure 10C) when compared to control littermates (Figure 10B). In contrast, the TA muscle S:W ratio was not significantly different between *Dbx1::Cre*;*ChAT$^{fl/fl}$* and control mice (Figure 10D). These EMG findings, in conjunction with physiological analyses, provide evidence that this locomotor task-dependent modulation of hindlimb muscle activity involves a $V0_C$ interneuron-mediated enhancement of motor neuron firing.

DISCUSSION

Motor circuits in the spinal cord are the final neural arbiters of movement. The force and duration of muscle contraction is determined by the pattern of motor neuron firing which, in turn, reflects the coordinated activity of spinal interneurons. Premotor interneurons provide excitatory and inhibitory commands and in addition are thought to modulate motor output during locomotor tasks. The identity, circuitry, and behavioral contributions of such modulatory neurons have, however, been difficult to decipher. Our analysis of $V0_C$ neuronal circuitry and physiology suggests that this small cluster of cholinergic premotor interneurons exerts a modulatory influence on locomotor behavior, providing an initial insight into the function of an intrinsic spinal modulatory system.

Identity and Diversity within the V0 Interneuron Cohort

Classical anatomical and physiological studies have provided evidence that spinal circuits dedicated to the control of motor output are constructed from a complex array of interneuron subtypes (Jankowska, 2001; Bannatyne et al., 2009). Most of

activity. Each point on the circle corresponds to a single action potential. The direction of the mean vector indicates the preferred firing phase of the neuron, and the length of the vector indicates the tuning of action potentials around their mean.

(F) Circular plot showing the preferred firing phases (position of mean vectors) for all FP-labeled $V0_{CG}$ neurons, revealing a significant correlation with ventral root bursting (Rayleigh test, $p < 0.05$). Data include neurons from *Pitx2::Cre*;*Thy1.lsl.YFP* (L1–L3 levels, closed circles; L4–L5 levels, open circles) and *Pitx2::Cre*;*vAChT* mice (L1–L3 levels, open triangles).

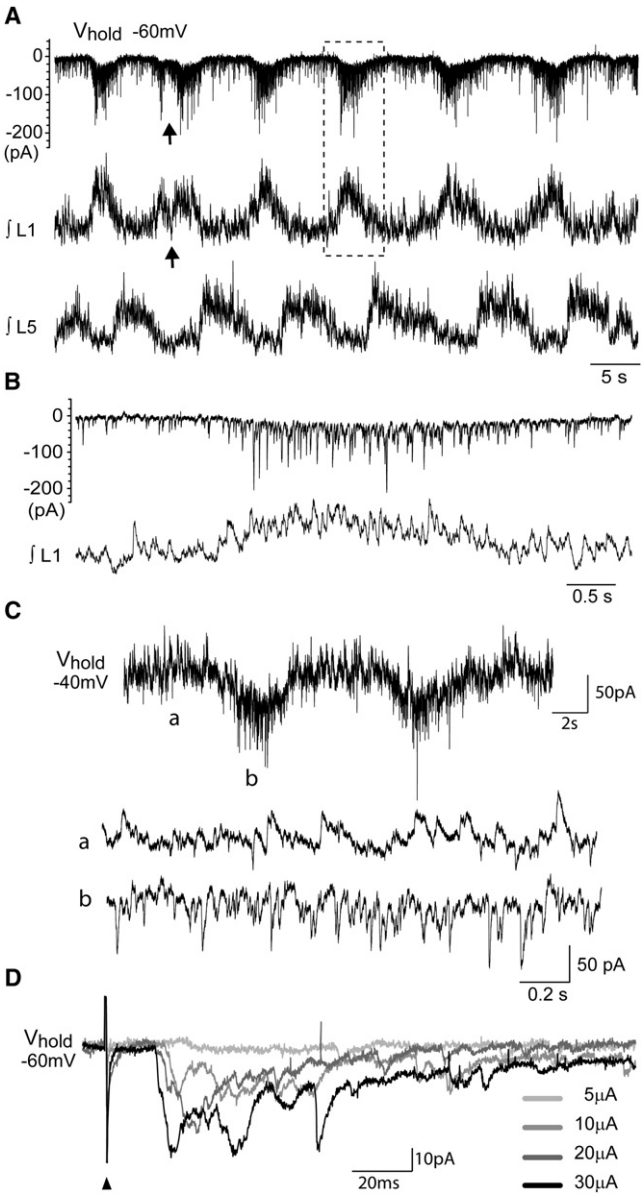

Figure 7. Synaptic Inputs to Pitx2$^+$ V0$_{CG}$ Interneurons

(A) Voltage-clamp recording of a *Thy1* FP-labeled V0$_{CG}$ neuron held at −60 mV (top trace) and rectified/integrated ventral root recordings (bottom traces) during drug-induced (NMDA 5 μM, 5-HT 10 μM, dopamine 50 μM) locomotor activity in a hemisected spinal cord preparation. The coupling between EPSCs recorded in this FP-labeled V0$_{CG}$ neuron and L1 ventral root activity is indicated by arrows.

(B) A volley of EPSCs recorded from the FP-labeled V0$_{CG}$ neuron in (A) (top trace) and a simultaneous ventral root burst (bottom trace). These data are outlined by the dotted box in (A).

(C) Voltage-clamp recordings of a *Thy1* FP-labeled V0$_{CG}$ neuron held at −40 mV reveal IPSCs throughout the locomotor cycle. Bottom two traces show data from the time points marked "a" and "b" in the top trace.

(D) Voltage-clamp recording of EPSCs evoked in a *Thy1* FP-labeled V0$_{CG}$ neuron by dorsal root stimulation (5–30 μA, 0.5 ms). Each trace is an average of five sweeps; arrowhead points to stimulus artifact.

these neurons derive from the four cardinal progenitor domains that subdivide the ventral half of the embryonic spinal cord (Jessell, 2000; Goulding, 2009), implying that a single progenitor domain gives rise to multiple interneuron subclasses. The p0 progenitor domain has been shown to give rise to two major groups of commissural inhibitory interneurons, V0$_V$ and V0$_D$ neurons (Pierani et al., 2001; Moran-Rivard et al., 2001; Lanuza et al., 2004). Our findings show that the V0$_V$ population can be further divided, in that it includes a small set of excitatory interneurons defined by the paired domain transcription factor Pitx2. And even this small Pitx2$^+$ neuronal subset can be fractionated into discrete V0$_C$ cholinergic and V0$_G$ glutamatergic populations. The program for specification of V0 interneuronal subtype identity therefore assigns discrete molecular identities to neuronal subsets that comprise only a few percent of the cardinal V0 cohort.

Equivalent diversification of other cardinal interneuron domains would imply the existence of over a hundred molecularly distinct ventral interneuron subtypes—a variety far greater than revealed by physiological or anatomical classification schemes. Nevertheless, there is precedent for the idea that an individual ventral progenitor domain can give rise to molecularly and functionally diverse neuronal subclasses. Renshaw interneurons are known to represent only ~10% of the total V1 interneuron population (Sapir et al., 2004; Alvarez et al., 2005), and Hb9$^+$ interneurons constitute an even smaller fraction of their cardinal interneuron class (Wilson et al., 2005). In addition, a dozen or more motor neuron subtypes derive from a single progenitor domain (Dasen et al., 2005), with individual motor pools often comprising only ~5% of total segmental motor neuron number (McHanwell and Biscoe, 1981).

By analogy with the mechanisms that direct motor neuron columnar and pool identity (Dasen et al., 2005; Dasen and Jessell, 2009) the specification of Pitx2$^+$ neurons within the V0 cohort could be initiated by a cell-intrinsic program of Hox protein repression. Notch signaling has been shown to direct binary differentiation of the cardinal V2 interneuron group into distinct glutamatergic V2a and GABAergic V2b subsets (Peng et al., 2007) and also contributes to neuronal diversification in the dorsal spinal cord (Mizuguchi et al., 2006). By extension, Notch signaling could drive the generation of discrete cholinergic and glutamatergic subtypes within the Pitx2$^+$ V0 interneuron group. Thus, sequential "winner-take-all" strategies of neuronal specification, initially a cell-intrinsic program of mutual Hox repression, and subsequently an intercellular program of Notch signaling, could underlie the progressive specification of neurons within the cardinal V0 population to a minority cholinergic V0$_C$ fate.

The analysis of Pitx2$^+$ V0 interneurons also reveals the extent of diversity in neurotransmitter phenotype and projection pattern that can emerge in the neuronal progeny of a single ventral progenitor domain. Most V0 interneurons exhibit GABAergic and/or glycinergic inhibitory character (Pierani et al., 2001; Lanuza et al., 2004; Moran-Rivard et al., 2001), but Pitx2$^+$ V0$_V$ interneurons are excitatory and use acetylcholine or glutamate as transmitters. Thus, a single ventral interneuron progenitor domain can give rise to interneurons of at least four different neurotransmitter phenotypes. Moreover many

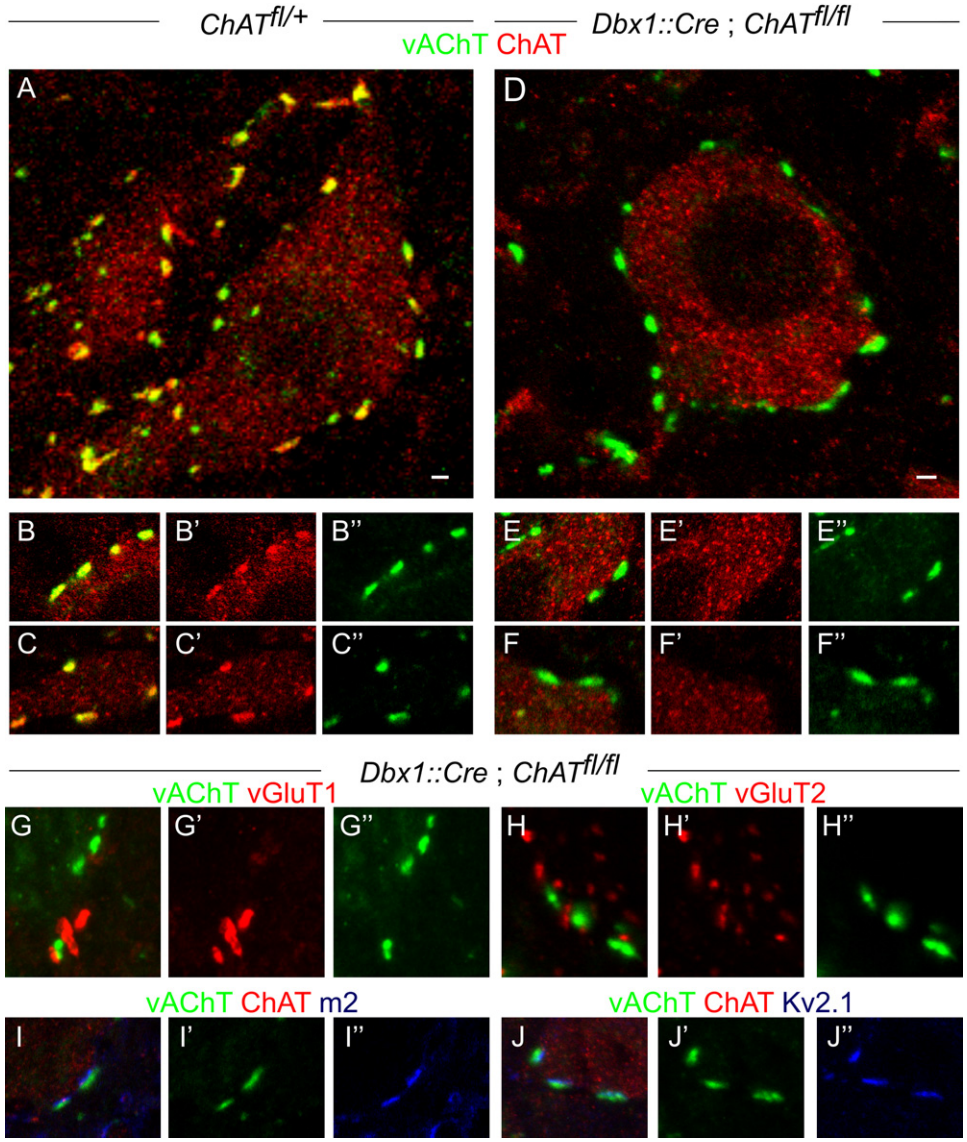

Figure 8. Genetically Programmed Elimination of ChAT from $V0_C$ Interneurons

(A–C″) Lumbar motor neurons in p24 *ChAT* $^{fl/+}$ mice express ChAT. C bouton terminals on motor neurons express both vAChT and ChAT.

(D–F″) Lumbar motor neurons in p24 *Dbx1::cre;ChAT* $^{fl/fl}$ mice express ChAT. Their C bouton inputs express vAChT, but not ChAT (n = 503 boutons from two p24 and three p60 mice).

(G–H″) In *Dbx1::cre;ChAT* $^{fl/fl}$ mice (p24 and p60), ChAT depleted C boutons do not express vGluT1 (G) or vGluT2 (H).

(I–J″) In *Dbx1::cre;ChAT* $^{fl/fl}$ mice (p60), m2 muscarinic receptors (I) and Kv2.1 channels (J) are clustered in alignment with $vAChT^+$, ChAT-deficient C boutons. Scale bar = 2 μm (A and D).

$Pitx2^+$ V0 interneurons appear to send axons ipsilaterally, whereas inhibitory V0 interneurons project their axons across the midline to innervate contralateral motor neurons (Pierani et al., 2001). Thus, progenitor provenance does not necessarily restrict the neurotransmitter phenotype or projection pattern of ventral interneurons.

Our findings also provide an insight into the contribution of neurotransmitter synthesis to the formation and maturation of interneuronal connections in mammalian CNS circuits. Selective elimination of ChAT from $V0_C$ neurons has no obvious influence on the maturation and organization of C bouton synapses with motor neurons. Similarly, elimination of ChAT from developing motor neurons and retinal amacrine neurons has no discernable anatomical impact on their development (Stacy et al., 2005; Myers et al., 2005). In contrast, glutamic acid decarboxylase (GAD) dependent synthesis and release of GABA appears to have a crucial role in the maturation of axonal arbors and synapses of GABAergic interneuron in visual cortex (Chattopadhyaya et al., 2007; Fagiolini and Hensch, 2000). The contribution of neurotransmitters to synaptic maturation in mammalian CNS

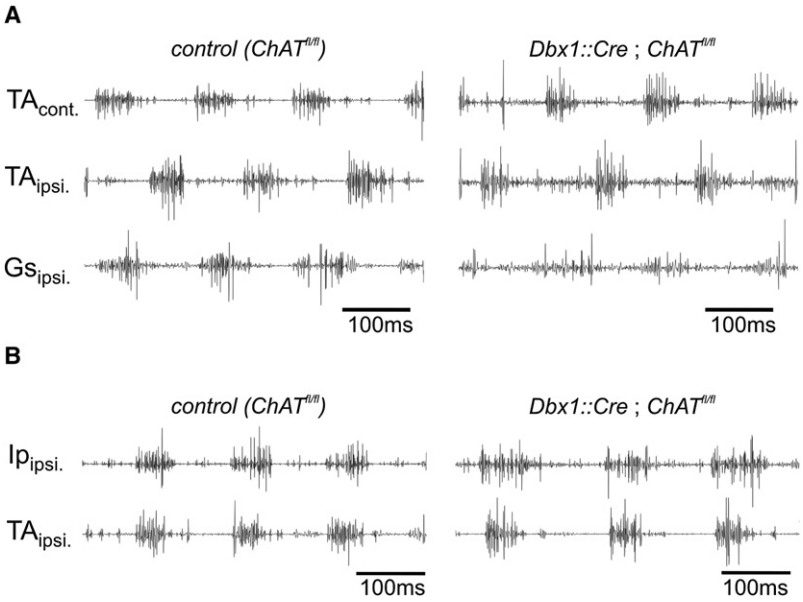

Figure 9. Preservation of Basic Locomotor Pattern in Mice with ChAT-Depleted V0$_C$ Neurons

(A) EMG recordings from the contralateral tibialis anterior (TA$_{cont}$, ankle flexor), ipsilateral TA (TA$_{ipsi.}$), and the ipsilateral gastrocnemius (Gs$_{ipsi.}$, ankle extensor) in control (*Chat*$^{fl/fl}$, left recordings; n = 7) and ChAT-depleted V0$_C$ neuron mice (*Dbx1::Cre*;*Chat*$^{fl/fl}$) (right recordings; n = 8 mice), during walking.

(B) In-phase activation of flexor muscles acting on different joints of the same leg (iliopsoas, Ip$_{ipsi}$, hip flexor and TA$_{ipsi}$, ankle flexor) is preserved in control (*Chat*$^{fl/fl}$) (left recordings; n = 5) and ChAT-depleted V0$_C$ neuron mice (*Dbx1::Cre*;*Chat*$^{fl/fl}$) (right recordings; n = 4), during walking.

circuits therefore differs as a function of neuronal subtype and transmitter status.

The Circuitry and Physiology of V0c Interneurons

V0$_C$ neurons are the sole source of C bouton synapses on spinal motor neurons. Their biophysical properties—slow tonic firing rates, broad action potentials, and large afterhyperpolarizing potentials—are typical of cholinergic and monoaminergic modulatory neurons in other regions of the mammalian CNS (Masuko et al., 1986; Li and Bayliss, 1998; Bennett et al., 2000). The organization of V0$_C$ neuronal projections is also suggestive of a modulatory role. In the lumbar spinal cord we estimate that motor neurons typically receive 80–100 C bouton contacts, and motor neurons outnumber V0$_C$ interneurons by a factor of ~10:1. Thus individual V0$_C$ neurons are likely to contribute ~1000 cholinergic synaptic contacts with target motor neurons, a divergence that places them in a pivotal position to modulate motor output.

During locomotor episodes, V0$_C$ neurons exhibit a rhythmic firing pattern that is tightly phase locked to the activity of segmentally-aligned motor neuron targets. Other studies have revealed considerably greater variability in the relative firing phases of broad populations of ventral glutamatergic interneurons (Butt and Kiehn, 2003; Butt et al., 2005). This presumably reflects the fact that this heterogeneous neuronal group is comprised both of last-order neurons that fire in register with motor bursts and upstream locomotor network interneurons that would not necessarily exhibit such tight linkage (McCrea and Rybak, 2008; Brownstone and Wilson, 2008). One small population of glutamatergic interneurons, defined by Hb9 expression (Wilson et al., 2005), fires in phase with segmental motor output (Hinckley et al., 2005), but its contributions to locomotor function are still unclear (Brownstone and Wilson, 2008; Kwan et al., 2009).

V0$_C$ neurons are unlikely to provide the major excitatory drive for motor neuron bursting. Rhythmic activity is maintained when V0 cholinergic output is eliminated in vivo and after blockade of muscarinic m2 receptors in vitro (Miles et al., 2007). More likely, the coordinated firing of V0c neurons and motor neurons reflects common rhythmic input from components of the core locomotor network. In support of this view, physiological analysis shows that rhythmic variation in the frequency of excitatory synaptic input to V0$_C$ interneurons coincides with activity in their aligned motor neuron targets. The spiking of V0$_C$ interneurons also matches the burst activity of segmentally aligned motor neurons and the cessation of activity in more caudally located "antagonist" motor neurons. We have not resolved whether individual V0$_C$ neurons innervate motor neurons in an indiscriminate manner or whether they respect flexor-extensor or pool-specific motor neuron characters. Nevertheless, our behavioral findings imply that descending or sensory pathways can activate spinal V0$_C$ neuronal circuits in a manner that enhances the firing rate of motor pools in a task-appropriate manner. We note that V0$_C$ neurons exhibit characteristics of "intrinsic" modulatory interneurons (Katz, 1995).

The physiology and connectivity of V0$_C$ neurons therefore suggests that they participate in spinal premotor circuits devoted to the modulation of motor output. Cholinergic signaling has previously been implicated in the generation of spinal motor rhythm (Cattaert et al., 1995; Quinlan et al., 2004; Cowley and Schmidt, 1994; Roberts et al., 2008; Hanson and Landmesser, 2003), although our findings imply that these activities are independent of V0$_C$ neurons. At embryonic stages, cholinergic influences on locomotor rhythm are mediated by the recurrent collaterals of motor neurons themselves (Myers et al., 2005). Thus, spinal cholinergic neurons involved in the generation of locomotor rhythm appear distinct from those involved in its modulation.

V0c Interneurons as Modulators of Locomotor Behavior

Locomotion in terrestrial vertebrates depends on the ability of neural circuits to regulate the function of individual limb muscles in a dynamic fashion during different locomotor tasks, even over the course of a single stride (Gillis and Biewener, 2001). Our findings provide genetic, physiological, and behavioral evidence for a task-dependent role for cholinergic V0$_C$ neurons in the modulation of mouse locomotor behavior—genetic manipulations that remove cholinergic C bouton signaling result in a significant impairment in the activation of the Gs muscle during swimming.

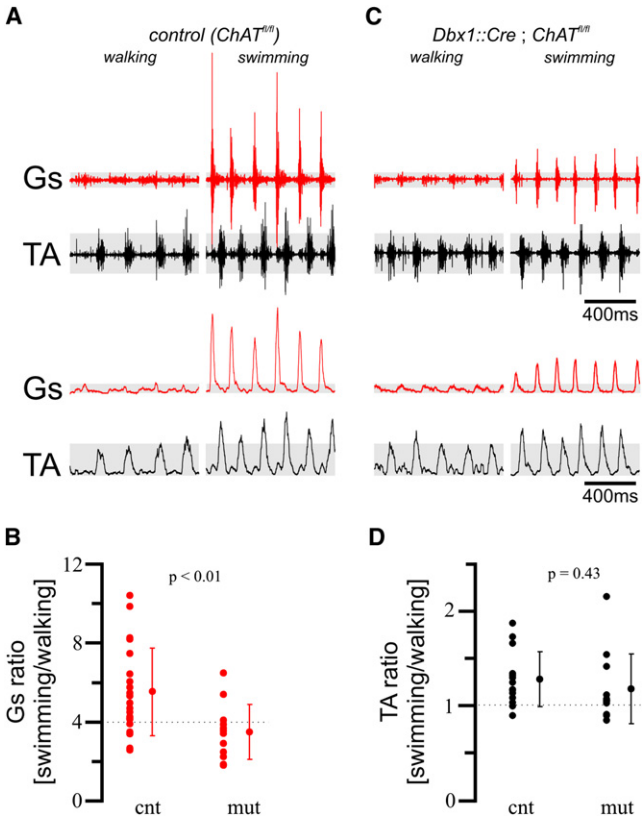

Figure 10. Task-Specific Impairment in Gastrocnemius Muscle Activation in Mice with ChAT-Depleted $V0_C$ Neurons

(A) EMG recordings from Gs (red) and TA (black) muscles during walking (left) and swimming (right), in control (*Chat*$^{fl/fl}$) mice. Raw and integrated EMG traces are shown.

(B) Ratio of Gs EMG amplitudes during walking and swimming in control WT (n = 8) and *Chat*$^{fl/fl}$ (n = 14 mice) and from $V0_C$ ChAT-deficient *Dbx1::Cre*; *Chat*$^{fl/fl}$ mice (n = 12 mice). The Gs data obtained from WT and *ChAT*$^{fl/fl}$ mice were pooled, since they were not statistically different (p = 0.13). The ratio of average peak values of Gs EMG activities during swimming and walking was significantly lower for *Dbx1::Cre*;*Chat*$^{fl/fl}$ mice compared to controls. Error bars indicate standard deviations.

(C) EMG recordings from Gs (red) and TA (black) muscles during walking (left) and swimming (right), in *Dbx1::Cre*;*Chat*$^{fl/fl}$ mice.

(D) Ratio of TA EMG amplitudes during walking and swimming in control *Chat*$^{fl/fl}$ (n = 12) and $V0_C$ ChAT-deficient *Dbx1::Cre*;*Chat*$^{fl/fl}$ mice (n = 14 mice). Error bars indicate standard deviations.

The demands of individual motor tasks—the transition from walking to swimming in our analysis—are likely to be transmitted to $V0_C$ interneurons via sensory or descending systems (Figure 11). Once activated, ACh release from the C bouton terminals of $V0_C$ neurons is likely to engage m2 muscarinic receptors on motor neurons, reducing spike afterhyperpolarization and enhancing motor neuron firing frequency (Miles et al., 2007). The impairment of Gs muscle activation observed after elimination of $V0_C$ neuronal output can therefore be explained by a failure to activate m2 muscarinic receptors at C bouton synapses. Nevertheless, the reduction in Gs muscle activation in V0 ChAT-depleted mice is incomplete. This could reflect the contribution of other modulatory systems that normally participate in the regulation of motor neuron firing rate (Liu et al., 2009; Krieger et al., 1998) or a compensatory change in the function of spinal networks after elimination of $V0_C$ cholinergic output (Myers et al., 2005; Stacy et al., 2005).

In the brain, cholinergic neurons have key roles in the attentional modulation of sensory processing streams (Giocomo and Hasselmo, 2007). In the owl optic tectum, the enhancement of neuronal responses to attended auditory and visual stimuli is mediated by cholinergic input from midbrain nuclei (Winkowski and Knudsen, 2008). In primate visual cortex, neuronal responses to images presented within attended receptive fields are elevated by activation of muscarinic signaling and reduced by muscarinic antagonists (Herrero et al., 2008). In one sense, the role of the spinal $V0_C$ cholinergic interneuron system in the task-appropriate gain control of selected motor neuron groups can be considered a motor attentional counterpart to these supraspinal cholinergic influences on sensory processing. Further analysis of the organization and function of $V0_C$ interneurons may therefore provide more general insight into the role of cholinergic modulatory systems throughout the mammalian CNS.

EXPERIMENTAL PROCEDURES

Differential Expression Screen

RNA was isolated from ventral and dorsal spinal cord tissue (n = 3 or 4 p8 mice for each sample) (Figure S1A) using the RNeasy Mini Kit (QIAGEN), and aRNA was synthesized with Ambion's MessageAmp aRNA Kit (Catalog # 1750) and Biotin 11-CTP and Biotin 16-UTP (Enzo). Affymetrix Gene chip Mouse Genome 430 2.0 Arrays were hybridized, and results were analyzed with the Gene Traffic software.

Generation of *Sox14::eGFP* and *vAChT.lsl.eGFP* Mice

The *Sox14::eGFP* and *vAChT.lsl.eGFP* (lsl: *loxP-stop-loxP* cassette) targeting vectors (details in Supplemental Experimental Procedures) were electroporated into mouse ES cells (129sv/ev) selected with G418, and homologous recombinants identified by Southern blot analysis. Targeted mouse ES cells were microinjected into blastocysts, and chimeric mice were crossed to C57BL/6J females. Additional mouse strains (Figure S8): *Dbx1::nlsLacZ* (Pierani et al., 2001), *Dbx1::Cre* (Bielle et al., 2005), *Pitx2::Cre* (*Pitx2δabc*^{creneo};Liu et al., 2003), *Thy1.lsl.YFP* (line15) (Buffelli et al., 2003; Bareyre et al., 2005), *Tau.lsl.mGFP-IRES-NLS-LacZ-pA* (Hippenmeyer et al., 2005), *Hb9::eGFP* (Wichterle et al., 2002), *ChAT*$^{fl/fl}$ (Misgeld et al., 2002; Buffelli et al., 2003).

Histochemistry

In situ hybridization histochemistry was performed on 15–20 μm cryostat sections as described (Dasen et al., 2005). Combined fluorescent in situ hybridization histochemistry/immunohistochemistry was performed on 15–20 μm cryostat sections.

Immunohistochemistry

Immunohistochemistry was performed as described (http://sklad.cumc.columbia.edu/jessell/resources/protocols.php) (Betley et al., 2009). Pitx2 antisera were generated in rabbit using the peptide MVPSAVTGVPGSSLC. Additional antibodies listed in Supplemental Experimental Procedures. Images were acquired on BioRad MRC 1024 or Zeiss LSM510 Meta confocal microscopes.

In Vitro Electrophysiology

Methods for recording from isolated spinal cord preparations have been described (Jiang et al., 1999). Further details provided in Supplemental Experimental Procedures. Data are reported as mean ± SE. Differences in means were compared using Student's t test. For analyses of interneuron firing phases, the phasing of individual action potentials was normalized to the onset

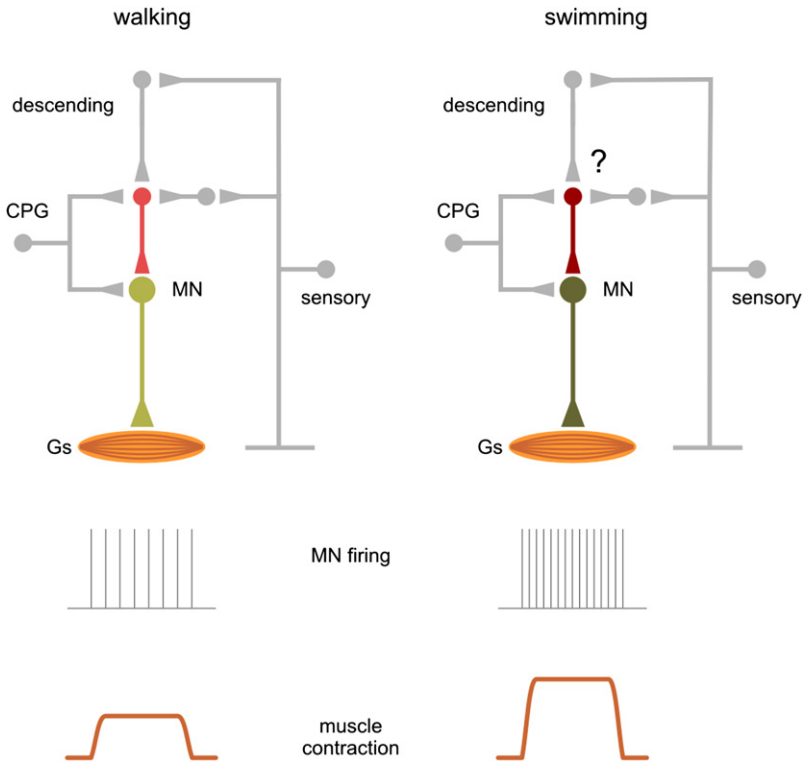

Figure 11. Intrinsic Neuromodulatory Role of $V0_C$ Interneurons

A model of the intraspinal circuitry and function of $Pitx2^+$ $V0_C$ interneurons. $V0_C$ neurons form numerous cholinergic C bouton synaptic contacts with motor neurons. They receive direct synaptic input from excitatory interneurons involved in the rhythmogenic central pattern generator (CPG) system, inputs from descending pathways, and indirect input from sensory afferents. During walking, the combined influence of these synaptic inputs results in a moderate level activation of the set of $V0_C$ neurons that innervate Gs motor neurons, which together with direct CPG input to motor neurons results in an intermediate rate of Gs motor neuron firing and a modest contraction of the Gs muscle. During swimming, a task-dependent change in the activity of sensory and descending pathways increases the level of activation of $V0_C$ neurons, activating muscarinic m2 receptors on motor neurons, enhancing Gs motor neuron firing frequency (Miles et al., 2007), and increasing the amplitude of Gs muscle contraction. For simplicity, we have not depicted direct descending modulatory inputs to motor neurons, which could contribute to the task-dependent modulation of Gs motor neuron activity. The question mark indicates the uncertain nature of the descending and/or sensory inputs that mediate the task-dependent regulation of $V0_C$ neuronal activity.

of rostral lumbar ventral root activity and circular plots generated where mean vector (arrow) direction represents the preferred firing phase and mean vector length (r) represents the concentration of action potentials around the mean (Butt et al., 2002). Relationships between preferred firing phases and ventral root activity were assessed using Rayleigh's test for uniformity (Kjaerulff and Kiehn, 1996; statistiXL software, Nedlands, WA, Australia). Values of $p < 0.05$ were considered significant.

Motor Behavioral Analysis

Adult mice were implanted with bipolar EMG recording electrodes (Pearson et al., 2005; Akay et al., 2006). EMG activities were recorded during free walking for ~20 min in a 78 cm × 4 cm Plexiglas runway. After walking trials, mice were placed in a tank with ~23°C water for ~2 min and EMG activity collected using Power1401 and Spike 2 (version 6.02, CED, Cambridge, UK) software and analyzed by Spike 2, Excel 2003, and statistiXL (version 1.8). Data are reported as mean ± SD and differences in distributions were tested by using the Student's t test (statistiXL). Values of $p < 0.05$ were considered significant.

SUPPLEMENTAL DATA

Supplemental Data include Supplemental Experimental Procedures and eight figures and can be found with this article online at http://www.cell.com/neuron/supplemental/S0896-6273(09)00846-0.

ACKNOWLEDGMENTS

We are grateful to Staceyann Doobar, Elizabeth Hwang, Qiaolian Liu, and Natasha Permaul for technical assistance; Barbara Han, Monica Mendelsohn, Jennifer Kirkland, and Susan Kales for help in the generation and upkeep of mice; and Susan Morton for antibody generation. We thank Lieven van der Veken for pseudorabies virus tracing, Silvia Arber for the *Tau.lsl.mGFP* line, Joshua Sanes for the $ChAT^{fl/fl}$ line, Alessandra Pierani for advice on *Dbx1::Cre* mice, Tord Hjalt for an aliquot of anti-Pitx2 antibody, and Apostolos Klinakis for DNA constructs. Frederic Bretzner, Christopher Henderson, John Martin, Joriene de Nooij, Sebastian Poliak, Victor Rafuse, and Keith Sillar provided helpful comments on the manuscript. L.Z. was supported by a Helen Hay Whitney Foundation Fellowship. T.A. is an HHMI research specialist. R.M.B. is supported by grants from ProjectALS and the Canadian Institutes of Health Research. G.B.M. is supported by grants from BBSRC UK, Project A.L.S., and Medical Research Scotland. J.F.M. is supported by NIH grants R01 DE/HD12324 and DE16329. T.M.J. is supported by grants from Project ALS, The Harold and Leila Mathers Foundation, The Wellcome Trust, NIH RO1 NS33245, and is an HHMI Investigator.

Accepted: October 16, 2009
Published: December 9, 2009

REFERENCES

Akay, T., Acharya, H.J., Fouad, K., and Pearson, K.G. (2006). Behavioral and electromyographic characterization of mice lacking EphA4 receptors. J. Neurophysiol. *96*, 642–651.

Al-Mosawie, A., Wilson, J.M., and Brownstone, R.M. (2007). Heterogeneity of V2-derived interneurons in the adult mouse spinal cord. Eur. J. Neurosci. *26*, 3003–3015.

Alvarez, F.J., and Fyffe, R.E. (2007). The continuing case for the Renshaw cell. J. Physiol. *584*, 31–45.

Alvarez, F.J., Jonas, P.C., Sapir, T., Hartley, R., Berrocal, M.C., Geiman, E.J., Todd, A.J., and Goulding, M. (2005). Postnatal phenotype and localization of spinal cord V1 derived interneurons. J. Comp. Neurol. *493*, 177–192.

Banfield, B.W., Kaufman, J.D., Randall, J.A., and Pickard, G.E. (2003). Development of pseudorabies virus strains expressing red fluorescent proteins: new tools for multisynaptic labeling applications. J. Virol. *77*, 10106–10112.

Bannatyne, B.A., Liu, T.T., Hammar, I., Stecina, K., Jankowska, E., and Maxwell, D.J. (2009). Excitatory and inhibitory intermediate zone interneurons in pathways from feline group I and II afferents: differences in axonal projections and input. J. Physiol. *587*, 379–399.

Barber, R.P., Phelps, P.E., Houser, C.R., Crawford, G.D., Salvaterra, P.M., and Vaughn, J.E. (1984). The morphology and distribution of neurons containing choline acetyltransferase in the adult rat spinal cord: an immunocytochemical study. J. Comp. Neurol. *229*, 329–346.

Bareyre, F.M., Kerschensteiner, M., Misgeld, T., and Sanes, J.R. (2005). Transgenic labeling of the corticospinal tract for monitoring axonal responses to spinal cord injury. Nat. Med. *11*, 1355–1360.

Bennett, B.D., Callaway, J.C., and Wilson, C.J. (2000). Intrinsic membrane properties underlying spontaneous tonic firing in neostriatal cholinergic interneurons. J. Neurosci. *20*, 8493–8503.

Betley, J.N., Wright, C.V.E., Kawaguchi, Y., Erdélyi, F., Szabó, G., Jessell, T.M., and Kaltschmidt, J.A. (2009). Stringent specificity in the construction of a GABAergic presynaptic inhibitory circuit. Cell *139*, 161–174.

Bielle, F., Griveau, A., Narboux-Nême, N., Vigneau, S., Sigrist, M., Arber, S., Wassef, M., and Pierani, A. (2005). Multiple origins of Cajal-Retzius cells at the borders of the developing pallium. Nat. Neurosci. *8*, 1002–1012.

Brownstone, R.M., and Wilson, J.M. (2008). Strategies for delineating spinal locomotor rhythm-generating networks and the possible role of Hb9 interneurones in rhythmogenesis. Brain Res. Rev. *57*, 64–76.

Brownstone, R.M., Jordan, L.M., Kriellaars, D.J., Noga, B.R., and Shefchyk, S.J. (1992). On the regulation of repetitive firing in lumbar motoneurones during fictive locomotion in the cat. Exp. Brain Res. *90*, 441–455.

Buffelli, M., Burgess, R.W., Feng, G., Lobe, C.G., Lichtman, J.W., and Sanes, J.R. (2003). Genetic evidence that relative synaptic efficacy biases the outcome of synaptic competition. Nature *424*, 430–434.

Butt, S.J., and Kiehn, O. (2003). Functional identification of interneurons responsible for left-right coordination of hindlimbs in mammals. Neuron *38*, 953–963.

Butt, S.J., Harris-Warrick, R.M., and Kiehn, O. (2002). Firing properties of identified interneuron populations in the mammalian hindlimb central pattern generator. J. Neurosci. *22*, 9961–9971.

Butt, S.J., Lundfald, L., and Kiehn, O. (2005). EphA4 defines a class of excitatory locomotor-related interneurons. Proc. Natl. Acad. Sci. USA *102*, 14098–14103.

Cattaert, D., Pearlstein, E., and Clarac, F. (1995). Cholinergic control of the walking network in the crayfish Procambarus clarkii. J. Physiol. (Paris) *89*, 209–220.

Cazalets, J.R., Borde, M., and Clarac, F. (1996). The synaptic drive from the spinal locomotor network to motoneurons in the newborn rat. J. Neurosci. *16*, 298–306.

Chattopadhyaya, B., Di Cristo, G., Wu, C.Z., Knott, G., Kuhlman, S., Fu, Y., Palmiter, R.D., and Huang, Z.J. (2007). GAD67-mediated GABA synthesis and signaling regulate inhibitory synaptic innervation in the visual cortex. Neuron *54*, 889–903.

Conradi, S., and Skoglund, S. (1969). Observations on the ultrastruture and distribution of neuronal and glial elements on the motoneuron surface in the lumbosacral spinal cord of the cat during postnatal development. Acta Physiol. Scand. Suppl. *333*, 5–52.

Cowley, K.C., and Schmidt, B.J. (1994). A comparison of motor patterns induced by N-methyl-D-aspartate, acetylcholine and serotonin in the in vitro neonatal rat spinal cord. Neurosci. Lett. *171*, 147–150.

Crone, S.A., Quinlan, K.A., Zagoraiou, L., Droho, S., Restrepo, C.E., Lundfald, L., Endo, T., Setlak, J., Jessell, T.M., Kiehn, O., and Sharma, K. (2008). Genetic ablation of V2a ipsilateral interneurons disrupts left-right locomotor coordination in mammalian spinal cord. Neuron *60*, 70–83.

Dasen, J.S., and Jessell, T.M. (2009). Hox networks and the origins of motor neuron diversity. Curr. Top. Dev. Biol. *88*, 169–200.

Dasen, J.S., Tice, B.C., Brenner-Morton, S., and Jessell, T.M. (2005). A Hox regulatory network establishes motor neuron pool identity and target-muscle connectivity. Cell *123*, 477–491.

de Leon, R., Hodgson, J.A., Roy, R.R., and Edgerton, V.R. (1994). Extensor- and flexor-like modulation within motor pools of the rat hindlimb during treadmill locomotion and swimming. Brain Res. *654*, 241–250.

Fagiolini, M., and Hensch, T.K. (2000). Inhibitory threshold for critical-period activation in primary visual cortex. Nature *404*, 183–186.

Fetcho, J.R., Higashijima, S., and McLean, D.L. (2008). Zebrafish and motor control over the last decade. Brain Res. Rev. *57*, 86–93.

Gillis, G.B., and Biewener, A.A. (2001). Hindlimb muscle function in relation to speed and gait: in vivo patterns of strain and activation in a hip and knee extensor of the rat (Rattus norvegicus). J. Exp. Biol. *204*, 2717–2731.

Giocomo, L.M., and Hasselmo, M.E. (2007). Neuromodulation by glutamate and acetylcholine can change circuit dynamics by regulating the relative influence of afferent input and excitatory feedback. Mol. Neurobiol. *36*, 184–200.

Goulding, M. (2009). Circuits controlling vertebrate locomotion: moving in a new direction. Nat. Rev. Neurosci. *10*, 507–518.

Grillner, S. (2006). Biological pattern generation: the cellular and computational logic of networks in motion. Neuron *52*, 751–766.

Hanson, M.G., and Landmesser, L.T. (2003). Characterization of the circuits that generate spontaneous episodes of activity in the early embryonic mouse spinal cord. J. Neurosci. *23*, 587–600.

Hellström, J. (2004). On the cholinergic C-bouton. PhD Thesis, Karolinska Institute, Stockholm, Sweden.

Hellström, J., Arvidsson, U., Elde, R., Cullheim, S., and Meister, B. (1999). Differential expression of nerve terminal protein isoforms in VAChT-containing varicosities of the spinal cord ventral horn. J. Comp. Neurol. *411*, 578–590.

Hellström, J., Oliveira, A.L., Meister, B., and Cullheim, S. (2003). Large cholinergic nerve terminals on subsets of motoneurons and their relation to muscarinic receptor type 2. J. Comp. Neurol. *460*, 476–486.

Herrero, J.L., Roberts, M.J., Delicato, L.S., Gieselmann, M.A., Dayan, P., and Thiele, A. (2008). Acetylcholine contributes through muscarinic receptors to attentional modulation in V1. Nature *454*, 1110–1114.

Hinckley, C.A., Hartley, R., Wu, L., Todd, A., and Ziskind-Conhaim, L. (2005). Locomotor-like rhythms in a genetically distinct cluster of interneurons in the mammalian spinal cord. J. Neurophysiol. *93*, 1439–1449.

Hippenmeyer, S., Vrieseling, E., Sigrist, M., Portmann, T., Laengle, C., Ladle, D.R., and Arber, S. (2005). A developmental switch in the response of DRG neurons to ETS transcription factor signaling. PLoS Biol. *3*, e159.

Hochman, S., and Schmidt, B.J. (1998). Whole cell recordings of lumbar motoneurons during locomotor-like activity in the in vitro neonatal rat spinal cord. J. Neurophysiol. *79*, 743–752.

Huang, A., Noga, B.R., Carr, P.A., Fedirchuk, B., and Jordan, L.M. (2000). Spinal cholinergic neurons activated during locomotion: localization and electrophysiological characterization. J. Neurophysiol. *83*, 3537–3547.

Hutchison, D.L., Roy, R.R., Hodgson, J.A., and Edgerton, V.R. (1989). EMG amplitude relationships between the rat soleus and medial gastrocnemius during various motor tasks. Brain Res. *502*, 233–244.

Jankowska, E. (2001). Spinal interneuronal systems: identification, multifunctional character and reconfigurations in mammals. J. Physiol. *533*, 31–40.

Jessell, T.M. (2000). Neuronal specification in the spinal cord: inductive signals and transcriptional codes. Nat. Rev. Genet. *1*, 20–29.

Jiang, Z., Carlin, K.P., and Brownstone, R.M. (1999). An in vitro functionally mature mouse spinal cord preparation for the study of spinal motor networks. Brain Res. *816*, 493–499.

Jordan, L.M., Liu, J., Hedlund, P.B., Akay, T., and Pearson, K.G. (2008). Descending command systems for the initiation of locomotion in mammals. Brain Res. Rev. *57*, 183–191.

Joshua, M., Adler, A., Mitelman, R., Vaadia, E., and Bergman, H. (2008). Midbrain dopaminergic neurons and striatal cholinergic interneurons encode the difference between reward and aversive events at different epochs of probabilistic classical conditioning trials. J. Neurosci. *28*, 11673–11684.

Katz, P.S. (1995). Intrinsic and extrinsic neuromodulation of motor circuits. Curr. Opin. Neurobiol. *5*, 799–808.

Kjaerulff, O., and Kiehn, O. (1996). Distribution of networks generating and coordinating locomotor activity in the neonatal rat spinal cord in vitro: a lesion study. J. Neurosci. *16*, 5777–5794.

Krieger, P., Grillner, S., and El Manira, A. (1998). Endogenous activation of metabotropic glutamate receptors contributes to burst frequency regulation in the lamprey locomotor network. Eur. J. Neurosci. *10*, 3333–3342.

Kwan, A.C., Dietz, S.B., Webb, W.W., and Harris-Warrick, R.M. (2009). Activity of Hb9 interneurons during fictive locomotion in mouse spinal cord. J. Neurosci. *29*, 11601–11613.

Lagerbäck, P.A., Ronnevi, L.O., Cullheim, S., and Kellerth, J.O. (1981). An ultrastructural study of the synaptic contacts of alpha-motoneurone axon collaterals. I. Contacts in lamina IX and with identified alpha-motoneurone dendrites in lamina VII. Brain Res. *207*, 247–266.

Lanuza, G.M., Gosgnach, S., Pierani, A., Jessell, T.M., and Goulding, M. (2004). Genetic identification of spinal interneurons that coordinate left-right locomotor activity necessary for walking movements. Neuron *42*, 375–386.

Lawrence, J.J. (2008). Cholinergic control of GABA release: emerging parallels between neocortex and hippocampus. Trends Neurosci. *31*, 317–327.

Li, Y.W., and Bayliss, D.A. (1998). Electrophysical properties, synaptic transmission and neuromodulation in serotonergic caudal raphe neurons. Clin. Exp. Pharmacol. Physiol. *25*, 468–473.

Li, W., Ochalski, P.A., Brimijoin, S., Jordan, L.M., and Nagy, J.I. (1995). C-terminals on motoneurons: electron microscope localization of cholinergic markers in adult rats and antibody-induced depletion in neonates. Neuroscience *65*, 879–891.

Liu, W., Selever, J., Lu, M.F., and Martin, J.F. (2003). Genetic dissection of Pitx2 in craniofacial development uncovers new functions in branchial arch morphogenesis, late aspects of tooth morphogenesis and cell migration. Development *130*, 6375–6385.

Liu, J., Akay, T., Hedlund, P.B., Pearson, K.G., and Jordan, L.M. (2009). Spinal 5-HT7 receptors are critical for alternating activity during locomotion: in vitro neonatal and in vivo adult studies using 5-HT7 receptor knockout mice. J. Neurophysiol. *102*, 337–348.

Lundfald, L., Restrepo, C.E., Butt, S.J., Peng, C.Y., Droho, S., Endo, T., Zeilhofer, H.U., Sharma, K., and Kiehn, O. (2007). Phenotype of V2-derived interneurons and their relationship to the axon guidance molecule EphA4 in the developing mouse spinal cord. Eur. J. Neurosci. *26*, 2989–3002.

Machacek, D.W., and Hochman, S. (2006). Noradrenaline unmasks novel self-reinforcing motor circuits within the mammalian spinal cord. J. Neurosci. *26*, 5920–5928.

Maskos, U., Molles, B.E., Pons, S., Besson, M., Guiard, B.P., Guilloux, J.P., Evrard, A., Cazala, P., Cormier, A., Mameli-Engvall, M., et al. (2005). Nicotine reinforcement and cognition restored by targeted expression of nicotinic receptors. Nature *436*, 103–107.

Masuko, S., Nakajima, Y., Nakajima, S., and Yamaguchi, K. (1986). Noradrenergic neurons from the locus ceruleus in dissociated cell culture: culture methods, morphology, and electrophysiology. J. Neurosci. *6*, 3229–3241.

McCrea, D.A., and Rybak, I.A. (2008). Organization of mammalian locomotor rhythm and pattern generation. Brain Res. Rev. *57*, 134–146.

McHanwell, S., and Biscoe, T.J. (1981). The localization of motoneurons supplying the hindlimb muscles of the mouse. Philos. Trans. R. Soc. Lond. B Biol. Sci. *293*, 477–508.

McLaughlin, B.J. (1972). Propriospinal and supraspinal projections to the motor nuclei in the cat spinal cord. J. Comp. Neurol. *144*, 475–500.

Mena-Segovia, J., Winn, P., and Bolam, J.P. (2008). Cholinergic modulation of midbrain dopaminergic systems. Brain Res. Rev. *58*, 265–271.

Miles, G.B., Hartley, R., Todd, A.J., and Brownstone, R.M. (2007). Spinal cholinergic interneurons regulate the excitability of motoneurons during locomotion. Proc. Natl. Acad. Sci. USA *104*, 2448–2453.

Misgeld, T., Burgess, R.W., Lewis, R.M., Cunningham, J.M., Lichtman, J.W., and Sanes, J.R. (2002). Roles of neurotransmitter in synapse formation: development of neuromuscular junctions lacking choline acetyltransferase. Neuron *36*, 635–648.

Mizuguchi, R., Kriks, S., Cordes, R., Gossler, A., Ma, Q., and Goulding, M. (2006). Ascl1 and Gsh1/2 control inhibitory and excitatory cell fate in spinal sensory interneurons. Nat. Neurosci. *9*, 770–778.

Moran-Rivard, L., Kagawa, T., Saueressig, H., Gross, M.K., Burrill, J., and Goulding, M. (2001). Evx1 is a postmitotic determinant of v0 interneuron identity in the spinal cord. Neuron *29*, 385–399.

Muennich, E.A., and Fyffe, R.E. (2004). Focal aggregation of voltage-gated, Kv2.1 subunit-containing, potassium channels at synaptic sites in rat spinal motoneurones. J. Physiol. *554*, 673–685.

Myers, C.P., Lewcock, J.W., Hanson, M.G., Gosgnach, S., Aimone, J.B., Gage, F.H., Lee, K.F., Landmesser, L.T., and Pfaff, S.L. (2005). Cholinergic input is required during embryonic development to mediate proper assembly of spinal locomotor circuits. Neuron *46*, 37–49.

Nagy, J.I., Yamamoto, T., and Jordan, L.M. (1993). Evidence for the cholinergic nature of C-terminals associated with subsurface cisterns in alpha-motoneurons of rat. Synapse *15*, 17–32.

Nicholson, L.F., Ma, L., and Goulding, M. (2001). Cloning and expression of Munc 30: a member of the paired -like homeodomain gene family. Cell Biol. Int. *25*, 351–365.

Orsal, D., Perret, C., and Cabelguen, J.M. (1986). Evidence of rhythmic inhibitory synaptic influences in hindlimb motoneurons during fictive locomotion in the thalamic cat. Exp. Brain Res. *64*, 217–224.

Pauli, W.M., and O'Reilly, R.C. (2008). Attentional control of associative learning—a possible role of the central cholinergic system. Brain Res. *1202*, 43–53.

Pearson, K.G., Acharya, H., and Fouad, K. (2005). A new electrode configuration for recording electromyographic activity in behaving mice. J. Neurosci. Methods *148*, 36–42.

Peng, C.Y., Yajima, H., Burns, C.E., Zon, L.I., Sisodia, S.S., Pfaff, S.L., and Sharma, K. (2007). Notch and MAML signaling drives Scl-dependent interneuron diversity in the spinal cord. Neuron *53*, 813–827.

Phelps, P.E., Barber, R.P., Houser, C.R., Crawford, G.D., Salvaterra, P.M., and Vaughn, J.E. (1984). Postnatal development of neurons containing choline acetyltransferase in rat spinal cord: an immunocytochemical study. J. Comp. Neurol. *229*, 347–361.

Pierani, A., Moran-Rivard, L., Sunshine, M.J., Littman, D.R., Goulding, M., and Jessell, T.M. (2001). Control of interneuron fate in the developing spinal cord by the progenitor homeodomain protein Dbx1. Neuron *29*, 367–384.

Polgár, E., Thomson, S., Maxwell, D.J., Al-Khater, K., and Todd, A.J. (2007). A population of large neurons in laminae III and IV of the rat spinal cord that have long dorsal dendrites and lack the neurokinin 1 receptor. Eur. J. Neurosci. *26*, 1587–1598.

Quinlan, K.A., Placas, P.G., and Buchanan, J.T. (2004). Cholinergic modulation of the locomotor network in the lamprey spinal cord. J. Neurophysiol. *92*, 1536–1548.

Roberts, A., Li, W.C., Soffe, S.R., and Wolf, E. (2008). Origin of excitatory drive to a spinal locomotor network. Brain Res. Rev. *57*, 22–28.

Roy, R.R., Hirota, W.K., Kuehl, M., and Edgerton, V.R. (1985). Recruitment patterns in the rat hindlimb muscle during swimming. Brain Res. *337*, 175–178.

Sapir, T., Geiman, E.J., Wang, Z., Velasquez, T., Mitsui, S., Yoshihara, Y., Frank, E., Alvarez, F.J., and Goulding, M. (2004). Pax6 and engrailed 1 regulate two distinct aspects of renshaw cell development. J. Neurosci. *24*, 1255–1264.

Semina, E.V., Reiter, R., Leysens, N.J., Alward, W.L., Small, K.W., Datson, N.A., Siegel-Bartelt, J., Bierke-Nelson, D., Bitoun, P., Zabel, B.U., et al. (1996). Cloning and characterization of a novel bicoid-related homeobox transcription factor gene, RIEG, involved in Rieger syndrome. Nat. Genet. *14*, 392–399.

Shefchyk, S.J., and Jordan, L.M. (1985). Motoneuron input-resistance changes during fictive locomotion produced by stimulation of the mesencephalic locomotor region. J. Neurophysiol. *54*, 1101–1108.

Smith, B.N., Banfield, B.W., Smeraski, C.A., Wilcox, C.L., Dudek, F.E., Enquist, L.W., and Pickard, G.E. (2000). Pseudorabies virus expressing enhanced green fluorescent protein: A tool for in vitro electrophysiological analysis of transsynaptically labeled neurons in identified central nervous system circuits. Proc. Natl. Acad. Sci. USA *97*, 9264–9269.

Stacy, R.C., Demas, J., Burgess, R.W., Sanes, J.R., and Wong, R.O. (2005). Disruption and recovery of patterned retinal activity in the absence of acetylcholine. J. Neurosci. *25*, 9347–9357.

VanderHorst, V.G., and Ulfhake, B. (2006). The organization of the brainstem and spinal cord of the mouse: relationships between monoaminergic, cholinergic, and spinal projection systems. J. Chem. Neuroanat. *31*, 2–36.

Wang, Z., Kai, L., Day, M., Ronesi, J., Yin, H.H., Ding, J., Tkatch, T., Lovinger, D.M., and Surmeier, D.J. (2006). Dopaminergic control of corticostriatal long-term synaptic depression in medium spiny neurons is mediated by cholinergic interneurons. Neuron *50*, 443–452.

Wess, J. (2003). Novel insights into muscarinic acetylcholine receptor function using gene targeting technology. Trends Pharmacol. Sci. *24*, 414–420.

Wichterle, H., Lieberam, I., Porter, J.A., and Jessell, T.M. (2002). Directed differentiation of embryonic stem cells into motor neurons. Cell *110*, 385–397.

Willis, W.D. (1971). The case for the Renshaw cell. Brain Behav. Evol. *4*, 5–52.

Wilson, J.M., Rempel, J., and Brownstone, R.M. (2004). Postnatal development of cholinergic synapses on mouse spinal motoneurons. J. Comp. Neurol. *474*, 13–23.

Wilson, J.M., Hartley, R., Maxwell, D.J., Todd, A.J., Lieberam, I., Kaltschmidt, J.A., Yoshida, Y., Jessell, T.M., and Brownstone, R.M. (2005). Conditional rhythmicity of ventral spinal interneurons defined by expression of the Hb9 homeodomain protein. J. Neurosci. *25*, 5710–5719.

Winkowski, D.E., and Knudsen, E.I. (2008). Distinct mechanisms for top-down control of neural gain and sensitivity in the owl optic tectum. Neuron *60*, 698–708.